Coordination of actuators for long heavy vehicle combinations using control allocation

Master's Thesis in Systems, Control and Mechatronics

PER NYMAN
KARIN UHLÉN

Department of Signals & Systems
Division of Automatic Control, Automation and Mechatronics
Chalmers University of Technology
Gothenburg, Sweden 2014

Master's Thesis EX024/2014

Abstract

Savings in for example, cost, emissions and road space, are factors that suggest the use of long heavy vehicles (LHV). These benefits come with the drawbacks of decreased stability and maneuverability. An active motion control system using more actuators is one possibility to improve the performance.

In this thesis, the coordination of motion actuators for LHV with several articulations joints is treated. The motion controller is based on a structure including control allocation, which is one approach to control an over-actuated system. The primary strength of the control allocation structure, is that only one system handles the motion control and the coordination of the actuators. Also, the desired motion request and actuator signals are separated. This gives the possibility to use the same control structure when the vehicle configuration is changed, only updating the settings in the control allocator.

The design of the control allocator is based on vehicle modeling using both the Newton and the Lagrange formulation. These approaches are evaluated to see which is the most convenient model to use for the design of control allocation, since no similar investigations have been done for LHV before.

The control structure is tested in a simulation environment and verified by three test scenarios. These are a split friction braking, a single lane change maneuver and a low speed 180° turn. Under the coordination of control allocation, all performance metrics for the test scenarios are improved when introducing more actuators. The conclusion drawn from the simulation is that, using control allocation together with more actuators, makes an LHV able to perform similar to a short heavy vehicle.

The control allocation structure makes a change of actuator configuration an easy procedure and it also gives the possibility to use it for an arbitrary LHV. The proposed control allocation structure is recommended for motion control of LHV in the future.

Keywords: long heavy vehicles, control allocation, motion control system, over-actuated system, split friction, single lane change, low speed maneuver

Acknowledgments

This master's thesis was carried out at the department of Chassis Strategies and Vehicle Analysis, at Volvo Group Trucks Technology (GTT) in Gothenburg. The time frame of the project was 20 weeks.

First of all we would like to thank our supervisor at GTT, Adjunct Professor Leo Laine, for your guidance and devotion. Your constant smile and encouraging words cheered us up many times. We would also like to extend a great deal of gratitude to Johan Eklöv at GTT, for your valuable inputs and collaboration.

To our supervisor and examiner at Chalmers, Associate Professor Jonas Fredriksson, thanks for all help and support during the project. Also thanks to Maliheh Sadeghi Kati at Chalmers, for always taking your time to help and giving us good material.

Finally, not to be forgotten, are all others at both Chalmers and GTT who have shown interest and helped us, it meant alot to us.

Thanks to you all, we have learned a lot and had a great time along the way.

Gothenburg, June 25, 2014
Per Nyman & Karin Uhlén

Contents

1

Introduction

In this thesis the coordination of motion actuators by the use of control allocation is studied for long heavy vehicle (LHV) combinations with several articulation joints. The focus is on analyzing whether it is possible to use this control structure for long heavy vehicles and how the control allocation design should look like. This section will give the some background and the motivation for using control allocation in this kind of vehicle application.

1.1 Background

The ambition in the development of heavy vehicles is to improve productivity, with increased volume and weight capability. At the same time there is need to decrease the environmental effect and still keep the same performance of the vehicle, [1]. The DUO^2-project, [2], is studying the so called modular concept and the transport-effectiveness of using longer vehicle combinations. In Figure 1.1 and Figure 1.2 two different vehicle combinations are shown. The standard two-unit tractor-semitrailer combination, Figure 1.1, have a gross combination weight (GCW), [3], of 40 tons, compared to the modular four-unit A-double combination, Figure 1.2, with a GCW of 80 tons. To transport the same amount of goods, the fuel consumption and emissions will be approximately 27 % less for the modular compared to the standard vehicle, according to [2]. Another benefit of using these longer combinations is that they occupy less road space to transport the same amount of goods, compared to the standard vehicles. This will help to reduce the congestion, which is a big problem in large parts in Europe. If the same performance could be obtained for a modular combination as a standard one, the vehicle have improved in many aspects.

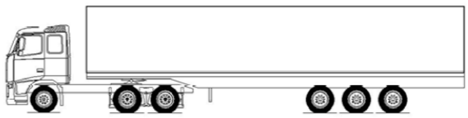

Figure 1.1: The tractor-semitrailer combination (originated from [1]).

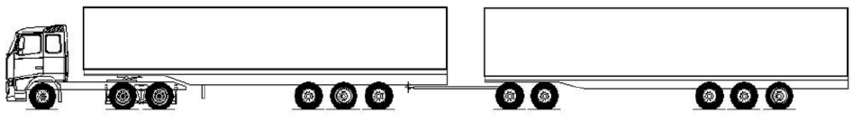

Figure 1.2: The A-double combination, tractor-semitrailer-dolly-semitrailer (originated from [1]).

By using longer vehicle combinations, both stability and maneuverability will in general be impaired, [1]. The ambition of keeping the same performance as the standard combinations, for example make the A-double behave as the tractor-semitrailer, puts higher demands on the vehicle's motion control system. To improve the performance of the vehicle, more actuators can be introduced. This is studied in [4] where a smart dolly, including steering and driving capability, is used in two different longer combinations. The result reveals that having a smart dolly with more controlled actuators benefits in both stability and maneuverability compared to the traditional configuration with passive dolly.

A problem when introducing more actuators is that the system may become over-actuated, which means that there are more motion actuators than controlled motions. To control the motion of an over-actuated system, there is a choice to be done in how to use the actuators in an appropriate way. The standard method for motion control of vehicles today, is to have many different strategies how to coordinate the actuator signals, depending on the demand and state of the vehicle. Another way of solving the decision-making is to divide the problem into two parts, referred to as control allocation, according to Figure 1.3. The driver generates a reference signal r, from which the control law computes the virtual control signal v needed for achieving the desired motion. The control allocation should then coordinate the actuator signals u to attain the needed virtual control.

The most common approach in today's research is to formulate the control allocator as a least square optimization problem, solved using standard interior point or active set methods. A study of the optimization solvers in the control allocation for a single-unit truck is done in [5]. The proposed control system shows performance similar to present systems in terms of vehicle stability. Real-time performance benchmarking also reveals that the system could be realizable in production vehicles in terms of execution time versus required sample time.

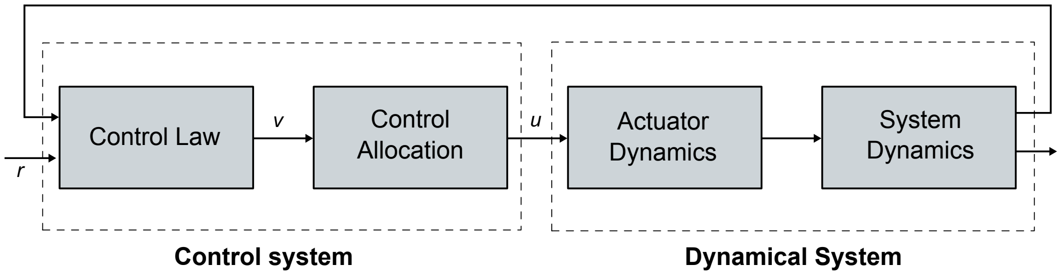

Figure 1.3: Closed loop system including a control system with control allocation.

Today, the motion control of heavy vehicles are decentralized. The brake system, steer system and drive system, are developed separately, which could be problematic in a assembled system to make them function together. The primary benefit of the control allocation structure is that it is only one system that handles the motion control and have access to the actuators. Many of the problems with a decentralized system can therefore be eliminated.

Another strength with the structure is that the desired virtual control, given from a higher level, is independent of the distribution of the signals to the actuators. This makes the system flexible and gives the possibility to use the same motion request for different kinds of vehicle configurations. There is also a possibility to optimize the actuator usage on-line by adapting the motion actuators to the current condition, for example the available tire force or the desired actuator usage. This makes it possible to optimize for example the energy consumption. The use of so called dynamic weighting in the problem formulation is done in [6], which shows considerable lower energy loss compared to static weighting. Another benefit with the control allocation structure is that the fault tolerance of the system can be increased, something that is studied in [7]. It is shown that the desired forces can be re-coordinated to the actuators still in function if there is a failure in some actuator.

Control allocation have been used in the stability control for passenger cars for some time [9], but in the area of heavy vehicles there are only a few reports, see e.g. [5] and [8]. In the area of long heavy vehicles, there are few reports addressing control allocation. For instance in [7], the yaw dynamics of a tractor-semitrailer is studied. The vehicle is stabilized by use of control allocation with the assumption of small angle approximation for both steer and articulation angles. In this thesis, the assumption of small angles is not used, and this is a significant simplification if it is used, especially for low speed maneuvers.

For articulated construction vehicles, control allocation have been used in [10]. A kinematic model is interpreted as a control allocator where the individual wheel drives are used as the only actuators. A kinematic model is a simpler model compared to a dynamic, and describes only the spatial and time-related variables. In this thesis, the forces of the vehicle is studied, which implies the need of a dynamic model. In [10], only one articulation joint is used and there is no steering applied to the wheels. In this thesis, several articulation joints and steer angles on the wheels are considered.

In [11], a balance control algorithm is implemented in order to improve the mobility of a leg-wheel hybrid structure where several articulation joints are present. The moment in the joints are the only actuators used to control the motion. There are some differences compared to this thesis; the articulation is yielding in the vertical direction, affected by the gravitational force, and no steering of the wheels is considered.

As shown in [1], there are a variety of prospective vehicle combinations that could be interesting for future utilization. A generic structure of the vehicle motion control is therefore desired, which gives the possibility to use it in many different configurations with only a few changes, which would save a lot of development time.

1.2 Purpose

The purpose of this thesis is to derive a general structure for control allocation in heavy vehicle combinations consisting of several units, which could be used for different maneuvers. The studied vehicle combination is general in a sense that the number of units, the number of axles on each unit, and where the actuators are placed is arbitrary.

As described in section 1.1 there is not much literature that describes how to formulate the optimization problem in the control allocator for a heavy vehicle with many units. Could the problem be formulated as a linear optimization problem? How are the articulation angles between the units handled? In summary, how should the optimization problem in the control allocator for a long heavy vehicle combination be formulated?

1.3 Limitations of scope

The delimitations used in this thesis are:

- The only actuators studied on each wheel are steering, braking and driving.
- Several assumptions in the modeling framework are used, such as a planar model, linear tires and no dynamics in the actuators. Details about specific assumptions are explained later on.
- For the verification of the control structure, no test on a real vehicle is performed. The verification is only done through simulation in Simulink and Volvo's *Virtual Truck Model* (VTM) library, [12].

- The solvers in the optimization problem and real-time performance are not studied.
- To validate the control allocation structure, two different vehicles and three specific scenarios are studied.

1.4 Test vehicles and scenarios

Two vehicle types are tested, the two-unit tractor-semitrailer combination shown in Figure 1.1, and the A-double combination, a four-unit tractor-semitrailer-dolly-semitrailer, see Figure 1.2. The tractor-semitrailer has acceptable performance in both high and low speed maneuvers, whereas the A-double combination has significantly worse performance, [1]. By adding extra actuators such as driving and steering on the dolly, the worse performance could be compensated for, [13]. The target for the A-double is to behave as close to the tractor-semitrailer as possible.

Three test scenarios are studied to validate the control allocation structure in different operating conditions. The first test is the so called split friction braking, where the friction on one side of the vehicle is reduced. To be able to drive straight during a braking from high speed, there is a need to counter-steer on the steerable axles. The second test is a single lane change maneuver meant to see the yaw stabilization at high speed. The last scenario studied, is a low speed maneuver driving through a 180 ° turn, like a roundabout turning. This test can evaluate the performance when both large steer and articulation angles are present.

The use of the test scenarios is to validate that different performance measures can be improved when adding extra actuators. The control allocator then has the potential of being a convenient structure for the motion control system when changing the configuration setup of a vehicle.

1.5 Outline of report

In chapter 2, two different vehicles models, including tire dynamics, are presented. These models form the basis to which the control allocation design is made. The control allocation problem is further described in chapter 3, together with the overall system design. The step from the vehicle model to the design of the control allocator is also presented. Chapter 4 describes the test scenarios for the simulations and performance measures to compare the different vehicle setups. The simulation results are then presented and discussed. Chapter 5 gives some concluding remarks and discussion of ideas for future work.

2

Modeling of a long heavy vehicle combination

To design a control allocator for a heavy vehicle combination an insight in the vehicle dynamics is needed to understand the impact of actuator forces to the dynamics. There are two main standard approaches in mechanical modeling of vehicles, the Newton's second law, [14], and the Lagrange equations, [15]. For heavy vehicles both modeling approaches can be found in literature, for example [7] uses the Newtonian formulation and [17] uses the Lagrangian formulation. The two different descriptions are equivalent to each other and which one is best to use is depending on the system configuration. To investigate which approach is most convenient in this context, both of the two modeling frameworks are studied.

The coordinate system used for the vehicle frame is defined in Figure 2.1. This is a right hand coordinate system, fixed in the center of gravity of the vehicle and is originated from the definition in ISO 8855. Each unit in the combination have its own coordinate frame according to this definition.

The models described in the next sections is only regarding planar motion. This means that the only interesting motions are the longitudinal, lateral and yaw motion. The longitudinal motion is defined along the x-axis, the lateral motions along the y-axis, and the rotation around the z-axis is referred to as the yaw motion, see Figure 2.1.

For convenience in the modeling formalism, three different variants of coordinate frames are used, see Figure 2.2. The tire coordinates are indicated with small letters like x and y. The vehicle coordinates, as used in Figure 2.1, are indicated with capital letters X and Y. The coordinates in a fix global frame are marked with an over-line like $\overline{X}$ and $\overline{Y}$.

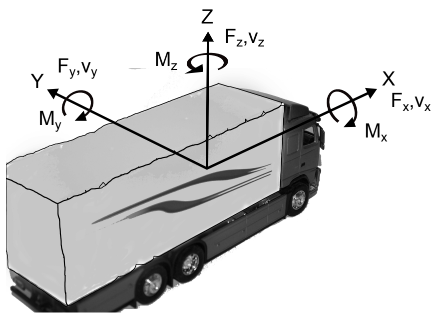

Figure 2.1: Vehicle coordinate frame (originated from [8]). Variables: v=velocity, F=force, M=moment.

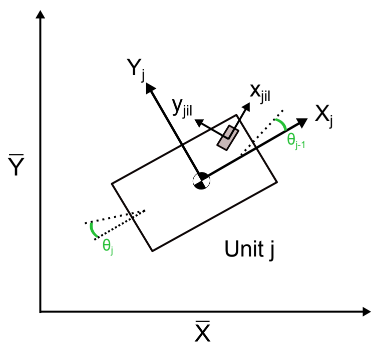

Figure 2.2: Coordinate definitions for unit j. The tire coordinates are depicted at axle i and on the left side (l) of the unit.

As mentioned above, the models will only consider planar motion, but there are some more assumptions used in the modeling; resistive forces like aerodynamic resistances are neglected, the units are considered as rigid masses and the left and right wheels have equal steer angle. There are also several assumptions regarding the tire dynamics which are discussed later.

To study the cornering dynamics of a vehicle in a convenient way, a so called single-track model is often used, [18]. In a single-track model, all tires on one axle is collapsed in to one virtual tire and the model captures the most important phenomena during cornering. To be able to study how individual wheel actuators affect the dynamics, a two-track model is instead needed, [14]. The modeling framework presented in this chapter is general in the sense of arbitrary number of units and actuators. For convenience and understanding, a two-track model of a A-double is considered and can be seen in Figure 2.3. Red forces in this figure are defined in the tire coordinate frame. Model parameters for the A-double are presented in Appendix A.3.

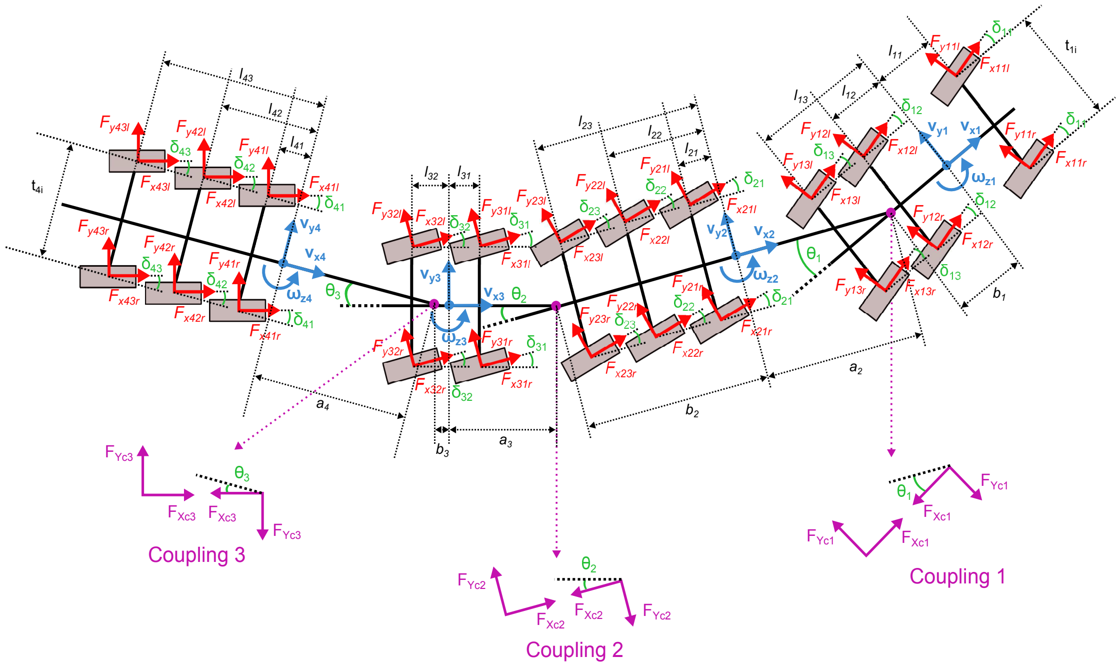

Figure 2.3: Two-track model of the A-double combination.

2.1 Tire dynamics

It is the forces generated in the contact between the tires and the road which affects the movement of the vehicle. The longitudinal forces are generated from torques applied to the wheels. The lateral forces are generated when the wheels are turned. A tire has a very complex dynamics and there are several tire models available, both empirical ,[18], and mathematical, [15]. A typical characteristic of a tire behavior is depicted as the blue line in Figure 2.4. Both the longitudinal (F_x) and lateral (F_y) forces on a tire shows these characteristics when the longitudinal slip (κ) or lateral slip (α) respectively is changed. The tire dynamics are described in more detail in the following sections.

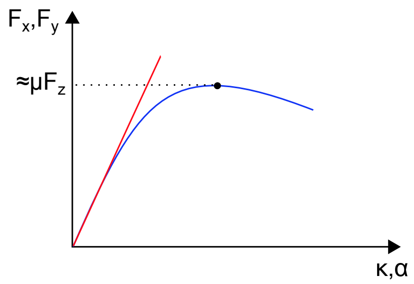

Figure 2.4: General force/slip relation of a tire.

2.1.1 Longitudinal forces

A simple and often sufficient model of the longitudinal dynamics is a linear tire model, depicted as the red line in Figure 2.4. For small values of the slip κ, this approximation is often sufficient. The linear tire model is defined as

$$F_x = C_x\kappa \tag{2.1}$$

where C_x is the longitudinal tire stiffness coefficient and κ is the so called "practical" longitudinal slip defined as

$$\begin{cases} \kappa = \frac{R\omega_w - v_x}{R\omega_w} \text{ (for a driven wheel)} \\ \kappa = \frac{R\omega_w - v_x}{v_x} \text{ (for a braked wheel)} \end{cases} \tag{2.2}$$

where R is the effective rolling radius of the wheel, ω_w is the rotational speed of the wheel and v_x is the longitudinal speed of the wheel hub in the tire coordinates. During acceleration or deceleration the difference $R\omega_w - v_x$ is nonzero and the slip will generate a force to move the vehicle according to (2.1). The use of two definitions for longitudinal slip eliminates the problem of division by zero.

An even more simplified tire model can be used if the longitudinal slip is assumed small and neglecting the rolling resistance and inertia of the tire. The longitudinal force F_x on a wheel is

$$F_x = \frac{T}{R} \tag{2.3}$$

where T is the applied wheel torque.

2.1.2 Lateral forces

To describe the lateral force generated by a tire in a easy way, a linear model is often used, depicted as the red line in Figure 2.4. As for the longitudinal model, the approximation is often sufficient for small slip values. The linear model is defined as

$$F_y = -C_\alpha\alpha \tag{2.4}$$

where C_α is the tire cornering stiffness and α is the side slip angle, shown in Figure 2.5. The side slip angle could be expressed as

$$\alpha = \beta - \delta \tag{2.5}$$

where β is the body side slip, defined as $arctan(\frac{v_Y}{v_X})$ in vehicle coordinates at the specific wheel position and δ is the steer angle of the wheel. The velocity v in Figure 2.5 is the total velocity of the wheel hub, which can be split into the longitudinal and lateral components v_X and v_Y respectively in the vehicle coordinates.

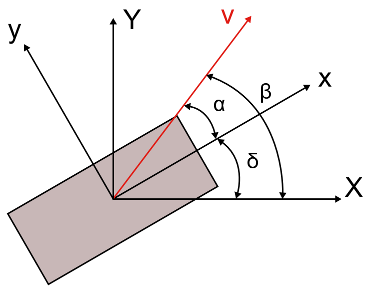

Figure 2.5: Definition of slip angles on a tire. Variables: v=wheel hub speed, α=side slip angle, β=body side slip angle at wheel position, δ=steer angle.

2.1.3 Combination of longitudinal and lateral forces

Many maneuvers often involve a combination of driving/braking and steering. During these conditions the tires are acting under so called combined slip, where the lateral and longitudinal slip are affecting each other.

A simple model to understand the behavior is the so called friction ellipse, [14]. The friction ellipse is expressed as

$$\left(\frac{F_y}{F_{y,max}}\right)^2 + \left(\frac{F_x}{F_{x,max}}\right)^2 = 1 \tag{2.6}$$

which states that the longitudinal and lateral forces cannot exceed their maximum values $F_{x,max}$ and $F_{y,max}$. If the friction level is simplified to be the same in all directions, the maximum values can be expressed as

$$F_{max} = \mu F_z \tag{2.7}$$

where μ is the friction level and F_z is the normal force on the wheel. This model will eliminate saturation of the tires in any direction.

A more sophisticated model of the tire is sometimes needed to fully understand the behavior of a tire. One such model that describes the combined slip behavior is presented in [15] and is shown in the subsequent equations. The so called "theoretical" tire slip in longitudinal and lateral directions are

$$\begin{cases} \sigma_x = \frac{\kappa}{1+\kappa} \\ \sigma_y = \frac{tan(\alpha)}{1+\kappa} \end{cases} \tag{2.8}$$

where κ and α are defined in (2.2) and (2.5) respectively. The expressions in (2.8) says that if the "practical" longitudinal slip, κ, is nonzero due to braking or driving, the longitudinal slip is changed, but the lateral slip will always decrease in the same direction, see lower equation in (2.8). The opposite, a change in the lateral slip angle, for example due to a change in the steer angle, will not affect the longitudinal slip. The total tire slip is defined as

$$\sigma = \sqrt{\sigma_x^2 + \sigma_y^2} \tag{2.9}$$

Defining the tire variable λ as

$$\lambda = 1 - \theta\sigma \tag{2.10}$$

where θ is a tire model parameter. The total forces which can be generated from a tire is

$$\begin{cases} F = \mu F_z \text{ (for a sliding tire)} \\ F = \mu F_z(1 - \lambda^3) \text{ (for a non-sliding tire)} \end{cases} \tag{2.11}$$

The components of the force in longitudinal and lateral direction can now be calculated

$$\begin{cases} F_x = F\frac{\sigma_x}{\sigma} \\ F_y = F\frac{\sigma_y}{\sigma} \end{cases} \tag{2.12}$$

As discussed above, when a positive or negative torque is applied to the wheels, the longitudinal slip will increase in the applied torque's direction, and the lateral slip decrease. This could be translated to the forces generated from the wheels according to (2.12). A practical example concluding the effects of combined slip could be during a maneuver when steering is used and the brakes are applied to maximum. This will result in lost steering ability, which means that the longitudinal forces will always dominate over the lateral forces.

2.2 Newton formulation

The derivation of motion equations by the use of Newton's second law are influenced by [13]. The equations of motion for each unit in a combination, for example the A-double in Figure 2.3, are

$$
\begin{aligned}
& m_j(\dot{v}_{xj} - v_{yj}\omega_{zj}) = \sum_{i=1}^{n_{aj}}(F_{Xjil} + F_{Xjir}) + F_{Xc(j-1)}cos(\theta_{(j-1)}) \\
& - F_{Yc(j-1)}sin(\theta_{(j-1)}) - F_{Xcj} \\
& m_j(\dot{v}_{yj} + v_{xj}\omega_{zj}) = \sum_{i=1}^{n_{aj}}(F_{Yjil} + F_{Yjir}) + F_{Xc(j-1)}sin(\theta_{(j-1)}) \\
& + F_{Yc(j-1)}cos(\theta_{(j-1)}) - F_{Ycj} \\
& J_j\dot{\omega}_{zj} = \sum_{i=1}^{n_{aj}}((F_{Yjil} + F_{Yjir})l_{ji} - (F_{Xjil} - F_{Xjir})\frac{t_{ji}}{2}) \\
& + F_{Yc(j-1)}cos(\theta_{(j-1)})a_j - F_{Ycj}b_j
\end{aligned}
\tag{2.13}
$$

where $j = 1 : n_u$ with n_u as the number of units in the combination, and $i = 1 : n_{aj}$ where n_{aj} is the number of axles on unit j, and l/r indicates left/right. For example, $n_u = 2$, $n_{aj} = [3\ 3]$ for the tractor-semitrailer (Figure 1.1) and $n_u = 4$, $n_{aj} = [3\ 3\ 2\ 3]$ for the A-double (Figure 1.2). The parameters m_j and J_j are the mass and yaw mass moment of inertia of unit j. The variables v_{xj}, v_{yj} and ω_{zj} are the longitudinal, lateral and yaw velocity of unit j, respectively. The articulation angles between the units are named θ_j for the coupling between unit j and unit $j+1$. The coupling forces F_{Xc0}, F_{Yc0}, F_{Xcn_u} and F_{Ycn_u} are all defined as zero. For ease of notation in this section, the lengths, such as l_{ji}, b_j and a_j, are defined as positive if they a placed in front of the unit's center of gravity (CoG) and negative if they are behind CoG.

The forces in (2.13) are expressed in the vehicle coordinate frame. The forces can instead be expressed in tire coordinates by a rotation matrix using steer angle

$$
\begin{pmatrix} F_{Xjir} & F_{Xjil} \\ F_{Yjir} & F_{Yjil} \end{pmatrix} = \begin{pmatrix} \cos(\delta_{ji}) & -\sin(\delta_{ji}) \\ \sin(\delta_{ji}) & \cos(\delta_{ji}) \end{pmatrix} \begin{pmatrix} F_{xjir} & F_{xjil} \\ F_{yjir} & F_{yjil} \end{pmatrix} \tag{2.14}
$$

The system in (2.13) together with (2.14) will form a system of equations with 3 x n_u equations. In these equations, the tire forces F_{xjil} and F_{xjir} are the inputs which can be controlled. The coupling forces F_{Xcj} and F_{Ycj} in between the units are forces which cannot be controlled directly and are therefor desired to be eliminated.

If the articulation joint between the units is modeled as a spring and damper in series, the coupling forces can directly be expressed as

$$
F_{Xcj} = c_j\Delta x_j + d_j\Delta v_{xj}, \ \ F_{Ycj} = c_j\Delta y_j + d_j\Delta v_{yj} \tag{2.15}
$$

where c_j and d_j are the spring and damper coefficient for the coupling, Δx_j, Δy_j, Δv_{xj} and Δv_{yj} are the difference in longitudinal position, lateral position, longitudinal velocity and lateral velocity in the coupling between unit j and $j+1$, respectively.

The equations in (2.15) inserted into the equations of motion will directly eliminate the coupling forces. Together with the models of the tires, the final system, suitable for the control allocation design, is found. The final form of the system equations is

$$\dot{x} = f(x) + g(x,u) \tag{2.16}$$

where x are the states v_{x1}, v_{y1}, ω_{z1},..., v_{xn_u}, v_{yn_u}, ω_{zn_u}, and the control inputs u are the wheel torque T or wheel speed ω_w (depending on tire model) on each wheel and steer angle δ on each axle.

2.3 Lagrange formulation

The motion equations can be derived from Lagrange's equations and the derivation in this section are based on [15].

Lagrange's equations are a system of differential equations in time, with generalized coordinates as variables. This system of equations is defined as

$$\frac{d}{dt}\frac{\partial T}{\partial \dot{q}_g} - \frac{\partial T}{\partial q_g} + \frac{\partial V}{\partial q_g} = Q_g, \qquad g = 1, 2, \ldots, M \tag{2.17}$$

where T and V is the total kinetic and potential energy of the system respectively, q_g are the generalized coordinates, Q_g are the generalized forces and M is the degrees of freedom. Due to the fact that only planar motion is considered the potential energy V is zero.

The choice of coordinates for a general combination is

$$q = (\overline{X}_1 \ \overline{Y}_1 \ \phi_1 \ \theta_1 \ \theta_2 \ \ldots \ \theta_{n_u-1}) \tag{2.18}$$

where $\overline{X}_1$ and $\overline{Y}_1$ are the positions in a global frame for the first unit's CoG, according to Figure 2.2, ϕ_1 is the yaw angle of the first unit, θ_j is the articulation angle between unit j and $j+1$ and n_u is the number of units in the combination.

With this choice of coordinates the motion equations will be defined in the global frame, but it is often more useful to have them defined in the vehicle frame. The relation between the velocity in the vehicle frame and the global frame is

$$\begin{pmatrix} \dot{X}_1 \\ \dot{Y}_1 \end{pmatrix} = \begin{pmatrix} \cos(\phi_1) & \sin(\phi_1) \\ -\sin(\phi_1) & \cos(\phi_1) \end{pmatrix} \begin{pmatrix} \dot{\overline{X}}_1 \\ \dot{\overline{Y}}_1 \end{pmatrix} \tag{2.19}$$

The motion equations can be transformed to vehicle coordinates, following the procedure in [15], using equation (2.19) and the chain rule

$$\begin{aligned}
\frac{\partial T}{\partial \dot{\bar{X}}_1} &= \frac{\partial T}{\partial \dot{X}_1}\frac{\partial \dot{X}_1}{\partial \dot{\bar{X}}_1} + \frac{\partial T}{\partial \dot{Y}_1}\frac{\partial \dot{Y}_1}{\partial \dot{\bar{X}}_1} = \frac{\partial T}{\partial \dot{X}_1}\cos(\phi_1) - \frac{\partial T}{\partial \dot{Y}_1}\sin(\phi_1) \\
\frac{\partial T}{\partial \dot{\bar{Y}}_1} &= \frac{\partial T}{\partial \dot{X}_1}\frac{\partial \dot{X}_1}{\partial \dot{\bar{Y}}_1} + \frac{\partial T}{\partial \dot{Y}_1}\frac{\partial \dot{Y}_1}{\partial \dot{\bar{Y}}_1} = \frac{\partial T}{\partial \dot{Y}_1}\sin(\phi_1) + \frac{\partial T}{\partial \dot{Y}_1}\cos(\phi_1) \\
\frac{\partial T}{\partial \phi} &= \frac{\partial T}{\partial \dot{X}_1}\frac{\partial \dot{X}_1}{\partial \phi} + \frac{\partial T}{\partial \dot{Y}_1}\frac{\partial \dot{Y}_1}{\partial \phi_1} = \frac{\partial T}{\partial \dot{X}_1}\dot{Y}_1 - \frac{\partial T}{\partial \dot{Y}_1}\dot{X}_1
\end{aligned} \tag{2.20}$$

The last relation uses

$$\frac{\partial \dot{X}_1}{\partial \phi_1} = \dot{Y}_1, \quad \frac{\partial \dot{Y}_1}{\partial \phi_1} = -\dot{X}_1 \tag{2.21}$$

According to [15], the final system of equations in the vehicle frame has the form

$$\begin{aligned}
&\frac{d}{dt}\frac{\partial T}{\partial \dot{X}_1} - \dot{\phi}_1\frac{\partial T}{\partial \dot{Y}_1} = Q_{X_1} \\
&\frac{d}{dt}\frac{\partial T}{\partial \dot{Y}_1} + \dot{\phi}_1\frac{\partial T}{\partial \dot{X}_1} = Q_{Y_1} \\
&\frac{d}{dt}\frac{\partial T}{\partial \dot{\phi}_1} - \dot{Y}_1\frac{\partial T}{\partial \dot{X}_1} + \dot{X}_1\frac{\partial T}{\partial \dot{Y}_1} = Q_{\phi_1} \\
&\frac{d}{dt}\frac{\partial T}{\partial \dot{\theta}_j} - \frac{\partial T}{\partial \theta_j} = Q_{\theta_j}
\end{aligned} \tag{2.22}$$

The kinetic energy of the system is defined as

$$T = \sum_{j=1}^{n_u} \frac{1}{2}m_j v_j^2 + \frac{1}{2}J_j\dot{\phi}_j \tag{2.23}$$

where v_j is the total velocity of unit j, $\dot{\phi}_j$, sometimes written as w_{zj}, is the yaw rate of unit j, m_j and J_j are the mass and yaw mass moment of inertia of unit j. It is important to note that the velocities v_j are the velocities in the vehicle frame.

The right hand side of (2.22) are the generalized forces which are inputs to the motion equations and can be controlled. The generalized forces are defined as

$$Q_g = \sum_{k=1}^{m} F_k \frac{\partial p_k}{\partial q_g} \tag{2.24}$$

where p_k are position vectors defining where the external forces F_k are applied to the system and m is the number of actuators. The external forces are calculated from the tire models in section 2.1 and are described more later.

When all parts in (2.22) are included, the final system of equations have the form

$$\dot{x} = f(x) + g(x,u) \tag{2.25}$$

where x are the states v_{x1}, v_{y1}, ω_{z1}, $\dot{\theta}_1$,..., $\dot{\theta}_{n_u-1}$, and the control inputs u are the wheel torque T or wheel speed ω_w (depending on tire model) on each wheel and steer angle δ on each axle.

3

Control Allocation

THIS CHAPTER introduces some of the theory for control allocation and shows the application for LHVs. The work in this section is based on [5], [8] and [20], with modifications for this application. In [20] a thorough introduction to control allocation can be found.

Control allocation is used to coordinate an over-actuated system with upper and lower limits in the actuator signals. Mathematically, control allocation solves a undetermined constrained system of equations.

3.1 Problem Formulation

Assume two formulations of a system that is desired to be equal

$$\begin{aligned} \dot{x} &= f(x) + v \\ \dot{x} &= f(x) + Bu \end{aligned} \tag{3.1}$$

where x is a vector of states, $f(x)$ is a nonlinear function, B is called the *control effectiveness matrix*, u is the *actuator input* or also called *true control input* and v is referred to as *virtual control input*. The state vector has $dim(x) = k$, the matrix $B \in \mathbb{R}^{k \times m}$, the actuator input vector has $dim(u) = m$ and the virtual control input vector has $dim(v) = k$. The first equation in (3.1) describes the desired form of the system, whereas the second equation describes what is available for control. To get a system where the two formulations are equal, the equation $v = Bu$ needs to be solved for the actuators inputs in u.

If the inequality $m > k$ holds, the system is called *over-actuated*. This means that the virtual control input v can be achieved in several ways because $v = Bu$ does not have a unique solution. When controlling these sorts of systems, the issue of non-uniqueness must be solved in some way. If it is not solved in a numerical way, there must be strategies on how to use the available actuators for a wide variety of motions, and this might be a strenuous task.

3.2 Optimization

One idea to address the problem of over-actuation is to map the virtual control vector v to the actuator input vector u through a constrained optimization problem

$$\begin{aligned} u &= \arg\min_{u\in\Omega} \|W_u(u_{des} - u)\|_2^2 \\ \Omega &= \arg\min_{\underline{u}\leq u\leq\bar{u}} \|W_v(Bu - v)\|_2^2 \end{aligned} \tag{3.2}$$

where the vector u_{des} is the desired actuator signals, W_u and W_v are diagonal weighting matrices used to prioritize certain actuator inputs or virtual control inputs respectively. This sort of problem is called sequential least squares problem (SLS) and can be simplified, [20], to

$$u = \arg\min_{\underline{u}\leq u\leq\bar{u}} (\|W_u(u_{des} - u)\|_2^2 + \gamma\|W_v(Bu - v)\|_2^2) \tag{3.3}$$

where γ is a weighting factor. This formulation is referred to as weighted least square problem (WLS). Solving (3.3) gives the vector of optimal control signals u. This idea to find u, is one common way to use *control allocation*.

The optimization problem in (3.3) is a quadratic programming problem and the literature for these types of problems is rich, both regarding solvers and theory. Earlier work have been done investigating this optimization problem for control allocation in a heavy vehicle application. In [5] it is stated that if the number of actuators are low, the active set method is a appropriate solver and if number of actuators are high the interior point method is a better choice. Both solvers can in general be used, but the best execution time achieved is making a switch from active set to interior point at around 25 actuator signals.

The parameter γ is a scaling parameter and is chosen by the designer. In general it is chosen to prioritize the $Bu - v$ term in the optimization higher, meaning that it is most important to find a solution that fulfills $Bu = v$. In the choice of γ, the inner relative dimension needs to be taken into consideration, which is important to avoid numerical instability [5].

The constraints in the problem formulation are due to the physical limitations of the actuators, and are set according to

$$u_{min} \leq u(t) \leq u_{max} \tag{3.4}$$

3.3 Vehicle application

For application in a vehicle, the virtual control input v to the system will be forces computed according to some control law to make the vehicle move as desired, see Figure 1.3. These forces are in this context called global forces and the solution to (3.3) will tell how much each actuator should generate to achieve them. The relation is described by the control effectiveness matrix B and is the input matrix to the state equations. Depending on which states are used in the modeling, the virtual control vector will be different, and therefore the B-matrix will have another form. Since the two modeling formalism shown in chapter 2 uses different states, several B-matrices can be derived.

The derived state equations in chapter 2 have the general form (2.25), repeated here for convenience

$$\dot{x} = f(x) + g(x,u) \tag{3.5}$$

The control allocation problem then have the nonlinear relationship

$$g(x,u) = v \tag{3.6}$$

and therefore the optimization in (3.3) cannot be used directly. Even though some attempts, see [21], have been made to solve (3.6) using nonlinear optimization, a more common approach is to linearize $g(x,u)$ to B, and end up with

$$Bu = v \tag{3.7}$$

which makes it possible to use (3.3). Usually this linearization include the approximation of small angles, in this case small steer and small articulation angles. Especially in low-speed maneuvers, this may not be a satisfactory assumption. Another possible approximation is to formulate the system as a Linear Parametric Varying (LPV) system, [22]. The idea is to update $g(x,u)$ in each sample with measurements to achieve a constant B-matrix in each sample according to

$$B(x,u)u = v \tag{3.8}$$

3.3.1 System overview

In Figure 3.1 an overview of the closed loop system design is shown, compare to Figure 1.3. The *Driver Model* represents a driver in the closed loop which acts depending on the driving situation and generates the reference signals to the control system. The *Target Generator* includes the control law to generate the desired global forces. The *Control Allocator* takes the global forces and coordinates the actuator signals in an optimal way. These signals are then sent to the motion control system in the *Vehicle*, which will deliver the motion that the driver commanded.

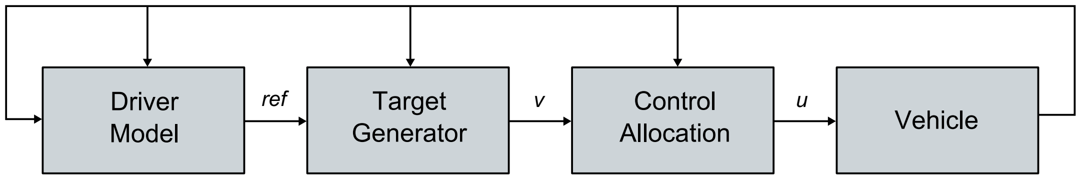

Figure 3.1: Overview of system design. Actuator dynamics are neglected and a driver model is included in the closed loop.

The job of the control allocator is to coordinate all the actuator signals in u, but there is one special case. During normal driving conditions the steering of the vehicle should behave as the driver expects. This means that the allocator does not have full control over the front steer angle signal, called δ_{11}. To make the allocator choose the steer angle that the driver demanded, feed-forward according to [8] is used. The feed-forward function, included in *Target Generator* in Figure 3.1, will generate targets for the allocator by setting, for example, the global forces F_Y and M_Z according to

$$\begin{aligned} F_Y &= 2C_\alpha \delta_{ref} \\ M_Z &= 2C_\alpha l \delta_{ref} \end{aligned} \tag{3.9}$$

where δ_{ref} is the steer angle that the driver expects. By using the same expressions in the B-matrix, the allocator will under normal conditions choose the provided steer angle due to the priority of the factor $Bu - v$ in the optimization problem.

There is a possibility for the front steer angle to deviate if the virtual control input could be better achieved. It is only during critical situations that the allocator will intervene and aid the driver with more or less steer angle. This extra steer angle is referred to as *angle overlay* and can be used to some degree, but not so much that the driver notices.

If it is known that the following units should be steered in a certain way, the desired steer angles should be added to the expression in the feed-forward, to always correlate to the terms in the B-matrix.

To help the allocator even more in finding the desired steer angle signals, calculated reference steer angles can also be used in the desired actuator usage vector u_{des}.

A summary of the signals sent to the control allocator block is depicted in Figure 3.2.

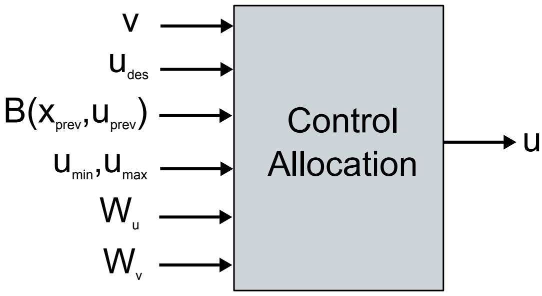

Figure 3.2: Illustration of the control allocation block where input and output signals are included.

3.3.2 Available actuators

The available actuators to control the vehicle are the drive/brake torques and steer angles on the tires. On a real vehicle drive and brake are two different actuators to generate torque. This is simplified to one term, which is defined for both positive (drive) and negative (brake) torque. There is individual brake/drive on each wheel. The longitudinal tire model used in the control allocation design is the simple model derived in (2.3) and repeated here for convenience

$$F_x = \frac{T}{R} \tag{3.10}$$

The linear lateral tire model in (2.4) and (2.5) is used in the control allocation design and could in compressed form be expressed as

$$F_y = f(x) + C_\alpha \delta \tag{3.11}$$

The actuators that is available for control of the vehicle motion is the torque T, positive or negative, and steer angle δ on the wheel. There is one torque for each wheel, and the steer angles on the same axle are assumed to be the same, which gives one steer actuator for each axle. A control input vector for a general combination could be expressed as

$$\begin{aligned} u_{generic} = (&T_{11l}\ T_{11r} \dots T_{1n_{a1}l}\ T_{1n_{a1}r}\ \delta_{11} \dots T_{n_u1l}\ T_{n_u1r} \dots \\ &T_{n_un_{anu}l}\ T_{n_un_{anu}r} \delta_{n_u1} \dots \delta_{n_un_{anu}})^\mathsf{T} \end{aligned} \tag{3.12}$$

where the notation is the same as used in chapter 2, using first index as unit, second index as axle and last index indicating left/right. The parameter n_u is the number of units in the combination, and n_{aj} is the number of axles on unit j. On the first unit, only the front axle is steered, which represent the case many in heavy vehicles today.

The control input vectors for the tested vehicle configurations are presented in Appendix A.1.

3.3.3 Derivation of B-matrix

For a general input vector as (3.12), the corresponding B-matrices for different variants of models will be derived in the following sections. The derivation is done using the computer algebra tool *Mathematica* and the notation follows the definition used in previous sections.

Newton model

The different actuators in (3.12) together with the equations of motion and the coupling model forms a system of equations on the general form (3.5).

From this system the part related to the global forces v could be extracted. The global forces for a general combination have the form

$$v_{N,alt1} = (F_{X_1}\ F_{Y_1}\ M_{Z_1}\ \ldots F_{Xn_u}\ F_{Yn_u}\ M_{Zn_u})^{\mathsf{T}} \tag{3.13}$$

With the v-vector in (3.13) and actuator signals in (3.12), the corresponding B-matrix have the form

$$B_{N,alt1} = \begin{pmatrix} B_{11} & 0 & \ldots & 0 \\ 0 & B_{22} & \ddots & \vdots \\ \vdots & \ddots & \ddots & 0 \\ 0 & \ldots & 0 & B_{n_u n_u} \end{pmatrix} \tag{3.14}$$

where the matrix components are

$$B_{11} = \begin{pmatrix} \frac{\cos(\delta_{11})}{R} & \frac{\cos(\delta_{11})}{R} & \dots & \frac{\cos(\delta_{1n_{a1}})}{R} & \frac{\cos(\delta_{1n_{a1}})}{R} & -2C_{\alpha 11}\sin(\delta_{11}) & \dots & -2C_{\alpha 1n_{1a}}\sin(\delta_{1n_{a1}}) \\ \frac{\sin(\delta_{11})}{R} & \frac{\sin(\delta_{11})}{R} & \dots & \frac{\sin(\delta_{1n_{a1}})}{R} & \frac{\sin(\delta_{1n_{a1}})}{R} & 2C_{\alpha 11}\cos(\delta_{11}) & \dots & 2C_{\alpha 1n_{a1}}\cos(\delta_{1n_{a1}}) \\ -\frac{t_{11}\cos(\delta_{11})-2l_{11}\sin(\delta_{11})}{2R} & \frac{t_{11}\cos(\delta_{11})+2l_{11}\sin(\delta_{11})}{2R} & \dots & -\frac{t_{1n_{a1}}\cos(\delta_{1n_{a1}})-2l_{1n_{a1}}\sin(\delta_{1n_{a1}})}{2R} & \frac{t_{1n_{a1}}\cos(\delta_{1n_{a1}})+2l_{1n_{a1}}\sin(\delta_{1n_{a1}})}{2R} & 2C_{\alpha 11}\cos(\delta_{11})l_{11} & \dots & 2C_{\alpha 1n_{a1}}\cos(\delta_{1n_a})l_{1n_{a1}} \end{pmatrix}$$

$$B_{22} = \begin{pmatrix} \frac{\cos(\delta_{21})}{R} & \frac{\cos(\delta_{21})}{R} & \dots & \frac{\cos(\delta_{2n_{a2}})}{R} & \frac{\cos(\delta_{2n_{a2}})}{R} & -2C_{\alpha 21}\sin(\delta_{21}) & \dots & -2C_{\alpha 2n_{a2}}\sin(\delta_{2n_{a2}}) \\ \frac{\sin(\delta_{21})}{R} & \frac{\sin(\delta_{21})}{R} & \dots & \frac{\sin(\delta_{2n_{a2}})}{R} & \frac{\sin(\delta_{2n_{a2}})}{R} & 2C_{\alpha 21}\cos(\delta_{21}) & \dots & 2C_{\alpha 2n_{a2}}\cos(\delta_{2n_{a2}}) \\ -\frac{t_{21}\cos(\delta_{21})-2l_{21}\sin(\delta_{21})}{2R} & \frac{t_{21}\cos(\delta_{21})+2l_{21}\sin(\delta_{21})}{2R} & \dots & -\frac{t_{2n_{a2}}\cos(\delta_{2n_{a2}})-2l_{2n_{a2}}\sin(\delta_{2n_{a2}})}{2R} & \frac{t_{2n_{a2}}\cos(\delta_{2n_{a2}})+2l_{2n_{a2}}\sin(\delta_{2n_{a2}})}{2R} & 2C_{\alpha 21}\cos(\delta_{21})l_{21} & \dots & 2C_{\alpha 2n_{a2}}\cos(\delta_{2n_{a2}})l_{2n_{a2}} \end{pmatrix}$$

$$B_{n_u n_u} = \begin{pmatrix} \frac{\cos(\delta_{n_u 1})}{R} & \frac{\cos(\delta_{n_u 1})}{R} & \dots & \frac{\cos(\delta_{n_u n_{an_u}})}{R} & \frac{\cos(\delta_{n_u n_{an_u}})}{R} & -2C_{\alpha n_u 1}\sin(\delta_{n_u 1}) & \dots & -2C_{\alpha n_u n_{an_u}}\sin(\delta_{n_u n_{an_u}}) \\ \frac{\sin(\delta_{n_u 1})}{R} & \frac{\sin(\delta_{n_u 1})}{R} & \dots & \frac{\sin(\delta_{n_u n_{an_u}})}{R} & \frac{\sin(\delta_{n_u n_{an_u}})}{R} & 2C_{\alpha n_u 1}\cos(\delta_{n_u 1}) & \dots & 2C_{\alpha n_u n_{an_u}}\cos(\delta_{n_u n_{an_u}}) \\ -\frac{t_{n_u 1}\cos(\delta_{n_u 1})-2l_{n_u 1}\sin(\delta_{n_u 1})}{2R} & \frac{t_{n_u 1}\cos(\delta_{n_u 1})+2l_{n_u 1}\sin(\delta_{n_u 1})}{2R} & \dots & -\frac{t_{n_u n_{an_u}}\cos(\delta_{n_u n_{an_u}})-2l_{n_u n_{an_u}}\sin(\delta_{n_u n_{an_u}})}{2R} & \frac{t_{n_u n_{an_u}}\cos(\delta_{n_u n_{an_u}})+2l_{n_u n_{an_u}}\sin(\delta_{n_u n_{an_u}})}{2R} & 2C_{\alpha n_u 1}\cos(\delta_{n_u 1})l_{n_u 1} & \dots & 2C_{\alpha n_u n_{an_u}}\cos(\delta_{n_u n_{an_u}})l_{n_u n_{an_u}} \end{pmatrix}$$

There is always a need to generate reference signals to all the global forces and sometimes it is not so easy to tell what these reference signals will be. In that case an option could be to skip some of the global forces and only keep the ones desired for control. An alternative setup of virtual control vector is

$$v_{N,alt2} = (F_{X_1}\ F_{Y_1}\ M_{Z_1} \dots M_{Zn_u})^{\intercal} \tag{3.15}$$

where only the ability to control the moments of the units behind the first unit is kept. This setup of virtual control vector will result in a general B-matrix as

$$B_{N,alt2} = \begin{pmatrix} B_{11} & 0 & \dots & 0 \\ 0 & B_{22} & \ddots & \vdots \\ \vdots & \ddots & \ddots & 0 \\ 0 & \dots & 0 & B_{n_u n_u} \end{pmatrix} \tag{3.16}$$

where the matrix components are

$$B_{11} = \begin{pmatrix} \frac{\cos(\delta_{11})}{R} & \frac{\cos(\delta_{11})}{R} & \cdots & \frac{\cos(\delta_{1n_{a1}})}{R} \\ \frac{\sin(\delta_{11})}{R} & \frac{\sin(\delta_{11})}{R} & \cdots & \frac{\sin(\delta_{1n_{a1}})}{R} \\ -\frac{t_{11}\cos(\delta_{11})-2l_{11}\sin(\delta_{11})}{2R} & \frac{t_{11}\cos(\delta_{11})+2l_{11}\sin(\delta_{11})}{2R} & \cdots & -\frac{t_{1n_{a1}}\cos(\delta_{1n_{a1}})-2l_{1n_{a1}}\sin(\delta_{1n_{a1}})}{2R} \end{pmatrix.}$$
$$\begin{matrix.} \frac{\cos(\delta_{1n_{a1}})}{R} & -2C_{\alpha 11}\sin(\delta_{11}) & \cdots & -2C_{\alpha 1n_{1a}}\sin(\delta_{1n_{a1}}) \\ \frac{\sin(\delta_{1n_{a1}})}{R} & 2C_{\alpha 11}\cos(\delta_{11}) & \cdots & 2C_{\alpha 1n_{a1}}\cos(\delta_{1n_{a1}}) \\ \frac{t_{1n_{a1}}\cos(\delta_{1n_{a1}})+2l_{1n_{a1}}\sin(\delta_{1n_{a1}})}{2R} & 2C_{\alpha 11}\cos(\delta_{11})l_{11} & \cdots & 2C_{\alpha 1n_{a1}}\cos(\delta_{1n_a})l_{1n_{a1}} \end{matrix} \right)$$

$$B_{22} = \Big(-\frac{t_{21}\cos(\delta_{21})-2l_{21}\sin(\delta_{21})}{2R} \quad \frac{t_{21}\cos(\delta_{21})+2l_{21}\sin(\delta_{21})}{2R} \quad \cdots \quad -\frac{t_{2n_{a2}}\cos(\delta_{2n_{a2}})-2l_{2n_{a2}}\sin(\delta_{2n_{a2}})}{2R}$$
$$\frac{t_{2n_{a2}}\cos(\delta_{2n_{a2}})+2l_{2n_{a2}}\sin(\delta_{2n_{a2}})}{2R} \quad 2C_{\alpha 21}\cos(\delta_{21})l_{21} \quad \cdots \quad 2C_{\alpha 2n_{a2}}\cos(\delta_{2n_{a2}})l_{2n_{a2}} \Big)$$

$$B_{n_u n_u} = \Big(-\frac{t_{n_u 1}\cos(\delta_{n_u 1})-2l_{n_u 1}\sin(\delta_{n_u 1})}{2R} \quad \frac{t_{n_u 1}\cos(\delta_{n_u 1})+2l_{n_u 1}\sin(\delta_{n_u 1})}{2R} \quad \cdots$$
$$-\frac{t_{n_u n_{an_u}}\cos(\delta_{n_u n_{an_u}})-2l_{n_u n_{an_u}}\sin(\delta_{n_u n_{an_u}})}{2R} \quad \frac{t_{n_u n_{an_u}}\cos(\delta_{n_u n_{an_u}})+2l_{n_u n_{an_u}}\sin(\delta_{n_u n_{an_u}})}{2R}$$
$$2C_{\alpha n_u 1}\cos(\delta_{n_u 1})l_{n_u 1} \quad \cdots \quad 2C_{\alpha n_u n_{an_u}}\cos(\delta_{n_u n_{an_u}})l_{n_u n_{an_u}} \Big)$$

The B-matrix in (3.16) will though have a problem. For example, during a brake-in maneuver only the actuators of the first unit will be activated, according to the first row in (3.16). This behavior is not desired, the brakes of the following units should also be used to get a short stopping distance. To activate the longitudinal actuators on the following units a modification of the B-matrix is done. By adding rows describing the coupling force between the units and telling the allocator to minimize these forces, the following units' actuators will also be chosen. It is only the coupling forces in the following units' direction that are interesting to minimize because these forces are causing the "jack-knife-effect" when there is an articulation angle present. For example, for the coupling between unit one and two the coupling force will be $F_{Xc1} = F_{X_1}cos(\theta_1) - F_{X_2}$. What reference the coupling forces will have in a driving situation is dependent on where driving axles are located and how driving capability should be divided between the units.

The virtual control vector v is modified to the form

$$v_{N,alt2,final} = (F_{X_1}\ F_{Y_1}\ M_{Z_1} \ldots M_{Zn_u}\ F_{Xc1}\ \ldots F_{Xc(n_u-1)})^{\intercal} \tag{3.17}$$

Rows describing the coupling forces are added to (3.16) and will form a new B-matrix obtained below. The symbol $\times$ is used to compress the notation and means that the procedure is repeated.

$$B_{N,alt2,final} = \begin{pmatrix} B_{11} & 0 & \dots & \dots & 0 \\ 0 & B_{22} & \ddots & & \vdots \\ \vdots & \ddots & \ddots & \ddots & 0 \\ \vdots & & \ddots & \ddots & 0 \\ 0 & \dots & \dots & 0 & B_{n_u n_u} \\ B_{c11} & B_{c12} & 0 & \dots & 0 \\ 0 & B_{c22} & B_{23} & \ddots & \vdots \\ \vdots & \ddots & \ddots & \ddots & \vdots \\ \vdots & & \times & \times & 0 \\ 0 & \dots & 0 & \times & B_{c(n_u-1)n_u} \\ 0 & \dots & \dots & \dots & 0 \end{pmatrix} \tag{3.18}$$

where the matrix components are

$$B_{11} = \begin{pmatrix} \frac{\cos(\delta_{11})}{R} & \frac{\cos(\delta_{11})}{R} & \dots & \frac{\cos(\delta_{1n_{a1}})}{R} \\ \frac{\sin(\delta_{11})}{R} & \frac{\sin(\delta_{11})}{R} & \dots & \frac{\sin(\delta_{1n_{a1}})}{R} \\ -\frac{t_{11}\cos(\delta_{11})-2l_{11}\sin(\delta_{11})}{2R} & \frac{t_{11}\cos(\delta_{11})+2l_{11}\sin(\delta_{11})}{2R} & \dots & -\frac{t_{1n_{a1}}\cos(\delta_{1n_{a1}})-2l_{1n_{a1}}\sin(\delta_{1n_{a1}})}{2R} \end{pmatrix.$$
$$\begin{matrix} \frac{\cos(\delta_{1n_{a1}})}{R} & -2C_{\alpha 11}\sin(\delta_{11}) & \dots & -2C_{\alpha 1n_{1a}}\sin(\delta_{1n_{a1}}) \\ \frac{\sin(\delta_{1n_{a1}})}{R} & 2C_{\alpha 11}\cos(\delta_{11}) & \dots & 2C_{\alpha 1n_{a1}}\cos(\delta_{1n_{a1}}) \\ \frac{t_{1n_{a1}}\cos(\delta_{1n_{a1}})+2l_{1n_{a1}}\sin(\delta_{1n_{a1}})}{2R} & 2C_{\alpha 11}\cos(\delta_{11})l_{11} & \dots & 2C_{\alpha 1n_{a1}}\cos(\delta_{1n_a})l_{1n_{a1}} \end{matrix}\right)$$

$$B_{22} = \Big(\; -\frac{t_{21}\cos(\delta_{21})-2l_{21}\sin(\delta_{21})}{2R} \quad \frac{t_{21}\cos(\delta_{21})+2l_{21}\sin(\delta_{21})}{2R} \quad \dots \quad -\frac{t_{2n_{a2}}\cos(\delta_{2n_{a2}})-2l_{2n_{a2}}\sin(\delta_{2n_{a2}})}{2R}$$
$$\frac{t_{2n_{a2}}\cos(\delta_{2n_{a2}})+2l_{2n_{a2}}\sin(\delta_{2n_{a2}})}{2R} \quad 2C_{\alpha 21}\cos(\delta_{21})l_{21} \quad \dots \quad 2C_{\alpha 2n_{a2}}\cos(\delta_{2n_{a2}})l_{2n_{a2}} \; \Big)$$

$$B_{n_u n_u} = \Big(\; -\frac{t_{n_u 1}\cos(\delta_{n_u 1})-2l_{n_u 1}\sin(\delta_{n_u 1})}{2R} \quad \frac{t_{n_u 1}\cos(\delta_{n_u 1})+2l_{n_u 1}\sin(\delta_{n_u 1})}{2R} \quad \dots$$
$$-\frac{t_{n_u n_{an_u}}\cos(\delta_{n_u n_{an_u}})-2l_{n_u n_{an_u}}\sin(\delta_{n_u n_{an_u}})}{2R} \quad \frac{t_{n_u n_{an_u}}\cos(\delta_{n_u n_{an_u}})+2l_{n_u n_{an_u}}\sin(\delta_{n_u n_{an_u}})}{2R}$$
$$2C_{\alpha n_u 1}\cos(\delta_{n_u 1})l_{n_u 1} \quad \dots \quad 2C_{\alpha n_u n_{an_u}}\cos(\delta_{n_u n_{an_u}})l_{n_u n_{an_u}} \; \Big)$$

$$B_{c11} = \Big(\; \frac{\cos(\delta_{11})}{R}\cos(\theta_1) \quad \frac{\cos(\delta_{11})}{R}\cos(\theta_1) \quad \dots \quad \frac{\cos(\delta_{1n_{a1}})}{R}\cos(\theta_1) \quad \frac{\cos(\delta_{1n_{a1}})}{R}\cos(\theta_1)$$
$$-2C_{\alpha 11}\sin(\delta_{11})\cos(\theta_1) \quad \dots \quad -2C_{\alpha 1n_{a1}}\sin(\delta_{1n_{a1}})\cos(\theta_1) \; \Big)$$

$$B_{c12} = \Big(\; -\frac{\cos(\delta_{21})}{R} \quad -\frac{\cos(\delta_{21})}{R} \quad \dots \quad -\frac{\cos(\delta_{2n_{a2}})}{R} \quad -\frac{\cos(\delta_{2n_{a2}})}{R} \quad 2C_{\alpha 21}\sin(\delta_{21}) \quad \dots \quad 2C_{\alpha 2n_{a2}}\sin(\delta_{2n_{a2}}) \; \Big)$$

$$B_{c22} = \Big(\; \frac{\cos(\delta_{21})}{R}\cos(\theta_2) \quad \frac{\cos(\delta_{21})}{R}\cos(\theta_2) \quad \dots \quad \frac{\cos(\delta_{2n_{a2}})}{R}\cos(\theta_2) \quad \frac{\cos(\delta_{2n_{a2}})}{R}\cos(\theta_2)$$
$$-2C_{\alpha 21}\sin(\delta_{21})\cos(\theta_2) \quad \dots \quad -2C_{\alpha 2n_{a2}}\sin(\delta_{2n_{a2}})\cos(\theta_2) \; \Big)$$

$$B_{c23} = \Big(\; -\frac{\cos(\delta_{31})}{R} \quad -\frac{\cos(\delta_{31})}{R} \quad \dots \quad -\frac{\cos(\delta_{3n_{a3}})}{R} \quad -\frac{\cos(\delta_{3n_{a3}})}{R} \quad 2C_{\alpha 31}\sin(\delta_{31}) \quad \dots \quad 2C_{\alpha 3n_{a3}}\sin(\delta_{3n_{a3}}) \; \Big)$$

$$B_{c(n_u-1)n_u} = \Big(\; -\frac{\cos(\delta_{(n_u-1)1})}{R} \quad -\frac{\cos(\delta_{(n_u-2)1})}{R} \quad \dots \quad -\frac{\cos(\delta_{(n_u-1)n_{a(n_u-1)}})}{R} \quad -\frac{\cos(\delta_{(n_u-1)n_{a(n_u-1)}})}{R}$$
$$2C_{\alpha(n_u-1)1}\sin(\delta_{(n_u-1)1}) \quad \dots \quad 2C_{\alpha(n_u-1)n_{a(n_u-1)}}\sin(\delta_{(n_u-1)n_{a(n_u-1)}}) \; \Big)$$

Lagrange model

The generalized forces Q_g are the inputs to the system of equations in (2.22). The generalized forces are defined in (2.24) and repeated here for convenience

$$Q_g = \sum_{k=1}^{m} F_k \frac{\partial p_k}{\partial q_g} \tag{3.19}$$

where p_k are position vectors defined where the external forces F_k are applied and m is the number of actuators. The external forces are generated by the tires and the position vectors will therefore define the tire positions. The procedure of defining the position vectors follows the outline in [17].

The left hand side of (3.19) is the virtual control input v. The external forces F_k represents the actuator signals in u. The right hand side of (3.19) describes how the actuator signals contributes to the virtual control. The B-matrix can therefore directly be extracted from (3.19).

As mentioned in section 2.3, the generalized coordinates are chosen to

$$q = (\overline{X}_1 \; \overline{Y}_1 \; \phi_1 \; \theta_1 \; \theta_2 \; \cdots \; \theta_{n_u}) \tag{3.20}$$

with the corresponding generalized forces

$$Q_g = (F_{X_1} \; F_{Y_1} \; M_{Z_1} \; M_{\theta_1} \ldots M_{\theta_{n_u}}) \tag{3.21}$$

When defining the position vectors it is convenient to define several coordinate systems and transformation matrices between them, see Figure 2.2 for the three coordinate frames used.

First a fixed global reference frame in which the vehicle moves

$$\begin{pmatrix} e_{\overline{X}} \\ e_{\overline{Y}} \end{pmatrix} \tag{3.22}$$

where $e_{\overline{X}}$ and $e_{\overline{Y}}$ are x and y coordinates respectively. Then define the coordinates in a vehicle frame fixed at the center of gravity of each unit j

$$\begin{pmatrix} e_{X_j} \\ e_{Y_j} \end{pmatrix} \tag{3.23}$$

The next step is to define transformation matrices between the coordinate systems. The first unit is rotated with its yaw angle relative to the global frame

$$\begin{pmatrix} e_{\overline{X}_1} \\ e_{\overline{Y}_1} \end{pmatrix} = \begin{pmatrix} \cos(\phi_1) & -\sin(\phi_1) \\ \sin(\phi_1) & \cos(\phi_1) \end{pmatrix} \begin{pmatrix} e_{X_1} \\ e_{Y_1} \end{pmatrix} \tag{3.24}$$

The second unit is rotated with the yaw angle plus the articulation angle relative to the global frame

$$\begin{pmatrix} e_{\overline{X}_2} \\ e_{\overline{Y}_2} \end{pmatrix} = \begin{pmatrix} \cos(\phi_1+\theta_1) & -\sin(\phi_1+\theta_1) \\ \sin(\phi_1+\theta_1) & \cos(\phi_1+\theta_1) \end{pmatrix} \begin{pmatrix} e_{X_2} \\ e_{Y_2} \end{pmatrix} \tag{3.25}$$

The transformation matrix for unit j is then

$$\begin{pmatrix} e_{\overline{X}_j} \\ e_{\overline{Y}_j} \end{pmatrix} = \begin{pmatrix} \cos(\phi_j+\theta_1+\theta_2+\cdots\theta_j) & -\sin(\phi+\theta_1+\theta_2+\cdots\theta_j) \\ \sin(\phi_j+\theta_1+\theta_2+\cdots\theta_j) & \cos(\phi_j+\theta_1+\theta_2+\cdots\theta_j) \end{pmatrix} \begin{pmatrix} e_{X_j} \\ e_{Y_j} \end{pmatrix} \tag{3.26}$$

The forces are rotated in a similar way using the same transformation matrices. The difference is that steered axles are rotated with an extra term due to the steering angle.

The position vectors for the tires on the left side of the vehicle can generally be defined as

$$p_{ji} = P_{CoG_j} + L_{ji}e_{X_j} + \frac{t_{ji}}{2}e_{Y_j} \tag{3.27}$$

and the position vectors for the tires on the right side of the vehicle can be defined as

$$p_{ji} = P_{CoG_j} + L_{ji}e_{X_j} - \frac{t_{ji}}{2}e_{Y_j} \tag{3.28}$$

where P_{CoG_j} defines the distance from the center of gravity of the first unit to the articulation point of unit j. Here L_{ji} is the distance, in x-coordinate, from the articulation point of unit j to the desired axle i, and t_{ji} is the track width at that axle. For example, the position vectors for two tires, left and right side, on the first axle on unit two

$$\begin{aligned} p_{21l} &= \overline{X}_1 + \overline{Y}_1 - b_1e_{X_1} - (a_2 + l_{21})e_{X_2} + \frac{t_{21}}{2}e_{Y_2} \\ p_{21r} &= \overline{X} + \overline{Y} - b_1e_{X_1} - (a_2 + l_{21})e_{X_2} - \frac{t_{21}}{2}e_{Y_2} \end{aligned} \tag{3.29}$$

see Figure 2.3 for notation of the lengths. A detailed example of calculating the generalized forces for a tractor-semitrailer is found in [17].

The generalized forces are, as mentioned, also the global forces used in the virtual control vector as

$$v = (F_{X_1}\ F_{Y_1}\ M_{Z_1}\ M_{\theta_1}\ \dots M_{\theta_j})^{\intercal} \tag{3.30}$$

Corresponding B-matrix can be written as

$$B_L = \begin{pmatrix} B_{11} & B_{12} & \dots & \dots & B_{1n_u} \\ 0 & B_{\theta_1 2} & B_{\theta_1 3} & \dots & B_{\theta_1 n_u} \\ 0 & 0 & B_{\theta_2 3} & \dots & B_{\theta_2 n_u} \\ 0 & 0 & 0 & \ddots & \vdots \\ 0 & \dots & \dots & 0 & B_{\theta_{n_u-1} n_u} \end{pmatrix} \tag{3.31}$$

where the first index in each component, indicates affected unit or articulation, and the second index indicates contribution unit. This structure of the B-matrix means that each unit or articulation joint is only affected by the units behind it. The first unit will be affected by the whole combination and the first row of (3.31) describes how each unit contributes to the virtual control inputs on unit one. That is, how each unit affect

F_{X_1}, F_{Y_1} and M_{Z_1}. Similarly, the second row describes how the virtual control input for M_{θ_1} is affected by the units behind the articulation joint. This is repeated up till $M_{\theta_{n_u-1}}$ which is only affected by the moments of the last unit of the combination. The elements in the first row of (3.31) are defined as

$$B_{11} = \left(\begin{matrix} \frac{\cos(\delta_{11})}{R} & \frac{\cos(\delta_{11})}{R} & \dots & \frac{\cos(\delta_{1n_{a1}})}{R} \\ \frac{\sin(\delta_{11})}{R} & \frac{\sin(\delta_{11})}{R} & \dots & \frac{\sin(\delta_{1n_{a1}})}{R} \\ -\frac{t_{11}\cos(\delta_{11})-2l_{11}\sin(\delta_{11})}{2R} & \frac{t_{11}\cos(\delta_{11})+2l_{11}\sin(\delta_{11})}{2R} & \dots & -\frac{t_{1n_{a1}}\cos(\delta_{1n_{a1}})-2l_{1n_{a1}}\sin(\delta_{1n_{a1}})}{2R} \end{matrix} \right.$$
$$\left. \begin{matrix} \frac{\cos(\delta_{1n_{a1}})}{R} & -2C_{\alpha 11}\sin(\delta_{11}) & \dots & -2C_{\alpha_{1n_{a1}}}\sin(\delta_{1n_{a1}}) \\ \frac{\sin(\delta_{1n_{a1}})}{R} & 2C_{\alpha 11}\cos(\delta_{11}) & \dots & 2C_{\alpha_{1n_{a1}}}\cos(\delta_{1n_{a1}}) \\ \frac{t_{1n_{a1}}\cos(\delta_{1n_{a1}})+2l_{1n_{a1}}\sin(\delta_{1n_{a1}})}{2R} & 2C_{\alpha 11}\cos(\delta_{11})l_{11} & \dots & 2C_{\alpha 1n_{a1}}\cos(\delta_{1n_{a1}})l_{1n_{a1}} \end{matrix} \right)$$

$$B_{12} = \left(\begin{matrix} \frac{\cos(\delta_{21}+\theta_1)}{R} & \frac{\cos(\delta_{21}+\theta_1)}{R} & \dots & \frac{\cos(\delta_{2n_{a2}}+\theta_1)}{R} & \frac{\cos(\delta_{2n_{a2}}+\theta_1)}{R} & -2C_{\alpha_{21}}\sin(\delta_{21}+\theta_1) \\ \frac{\sin(\delta_{21}+\theta_1)}{R} & \frac{\sin(\delta_{21}+\theta_1)}{R} & \dots & \frac{\sin(\delta_{2n_{a2}}+\theta_1)}{R} & \frac{\sin(\delta_{2n_{a2}}+\theta_1)}{R} & 2C_{\alpha 21}\cos(\delta_{21}+\theta_1) \\ \frac{-L_{21l}}{2R} & \frac{L_{21r}}{2R} & \dots & -\frac{L_{2n_{a2}l}}{2R} & \frac{L_{2n_{a2}r}}{2R} & -2C_{\alpha 21}L_{21} \end{matrix} \right.$$
$$\left. \begin{matrix} \dots & -2C_{\alpha 21}\sin(\delta_{2n_{a2}}+\theta_1) \\ \dots & 2C_{\alpha 21}\cos(\delta_{2n_{a2}}+\theta_1) \\ \dots & -2C_{\alpha 2n_{a2}}L_{2n_{a2}} \end{matrix} \right)$$

$$B_{1n_u} = \left(\begin{matrix} \frac{\cos(\delta_{n_u1}+\theta_1+\ldots+\theta_{n_u-1})}{R} & \dots & \frac{\cos(\delta_{n_un_{an_u}}+\theta_1+\ldots+\theta_{n_u-1})}{R} & -2C_{\alpha n_u1}\sin(\delta_{n_u1}+\theta_1+\ldots+\theta_{n_u-1}) \\ \frac{\sin(\delta_{n_u1}+\theta_1+\ldots+\theta_{n_u-1})}{R} & \dots & \frac{\sin(\delta_{n_un_{an_u}}+\theta_1+\ldots+\theta_{n_u-1})}{R} & 2C_{\alpha n_u1}\cos(\delta_{n_u1}+\theta_1+\ldots+\theta_{n_u-1}) \\ \frac{L_{n_u1}}{2R} & \dots & -\frac{L_{n_un_{an_u}r}}{2R} & -2C_{\alpha n_u1}L_{n_u1} \end{matrix} \right.$$
$$\left. \begin{matrix} \dots & -2C_{\alpha n_un_{an_u}}\sin(\delta_{n_un_{an_u}}+\theta_1+\ldots+\theta_{n_u-1}) \\ \dots & 2C_{\alpha n_un_{an_u}}\cos(\delta_{n_un_a}+\theta_1+\ldots+\theta_{n_u-1}) \\ \dots & -2C\alpha n_un_{an_u}L_{n_un_{an_u}} \end{matrix} \right)$$

where $j = 1 : n_u$ with n_u as the number of units in the combination, and $i = 1 : n_{aj}$ where n_{aj} is the number of axles on unit j. The lengths $L_{jil/r}$ are defined from the CoG of the first unit, to the left (l) or right (r) side of axle i on unit j. If no index of side (l/r) is used, it means middle position of the axle. For the parts in (3.31) describing the articulation moments, two example of the elements are given as

$$B_{\theta_12} = \begin{pmatrix} -\frac{L\theta_{1,21l}}{2R} & \dots & \frac{L\theta_{1,2n_ar}}{2R} & -2C_{\alpha 11}L\theta_{1,21} & \dots & -2C_{\alpha 1n_{a1}}L\theta_{1,2n_a} \end{pmatrix}$$

$$B_{\theta_{n_u-1}n_u} = \begin{pmatrix} -\frac{L\theta_{n_u-1,n_u1l}}{2R} & \dots & \frac{L\theta_{n_u-1,n_un_ar}}{2R} & -2C_{\alpha n_u1}L\theta_{n_u-1,n_u1} & \dots & -2C_{\alpha n_un_{an_u}}L\theta_{n_u-1,n_un_a} \end{pmatrix}$$

where the same notation is used as above, but instead the lengths $L_{\theta,jil/r}$ are defined from the articulation using the angle θ, to left (l) or right (r) side of axle i on unit j.

The complete B-matrix for the A-double combination, with maximum number of actuators, is presented in Appendix A.2.

4

Simulation

This chapter describes the test setups and results from the simulations. There are no validation made in a real truck because of time and cost constraints, but also due to the convenience of testing in a simulation environment. The simulations are performed on both the tractor-semitrailer combination, Figure 1.1, and the A-double combination, Figure 1.2.

4.1 Test scenarios

To evaluate the control allocation structure three test scenarios are performed. These scenarios are chosen to test the structure in different operating conditions, from high to low speed and where both small and large steer and articulation angles are present.

In [23], technical characteristics, denoted performance based characteristics (PBC), are defined for LHVs. These PBC are listed to set requirements on longer combinations for safety purposes. Lateral performance measures are the main focus in these test scenarios.

4.1.1 Split friction braking

This test scenario is carried out as follows. The vehicle is traveling at high speed facing an area with different friction levels on left and right side. When the whole combination is on this ground, the vehicle performs a braking to standstill while trying to keep the straight path. The brake capabilities are reduced on the low friction side, but not on the high friction side. If maximum brake force is applied the combination will slide out or it may "jack-knife" depending on how the brake forces are distributed. This behavior can be reduced or avoided if steering is applied to counteract the moment created by the uneven braking. The test is carried out in a closed loop, where a driver model applies a steer action to the front axle trying to keep the path.

To evaluate the performance of the braking maneuver, one of the most important performance metrics is the stopping distance. The objective of this measure is to ensure that the vehicle will decelerate and stop at an appropriate distance to avoid collisions.

Stopping distance is defined as, [23]: *"The distance traveled by a fully laden vehicle combination during straight line full braking from a certain initial speed and it is measured from the first pedal contact or when the brake request is sent from automatic braking until the vehicle comes to a standstill at a certain friction level."*

To see how well the vehicle keeps the straight path during the maneuver, the maximum lateral off-tracking is also evaluated.

Lateral off-tracking in the split friction maneuver is defined as: *"The maximum lateral offset from the original straight path to the center of the most severely off-tracking axle of any unit during the brake-in maneuver."*

Another relevant measure to study is the deceleration during the maneuver. The average longitudinal deceleration is calculated during the braking. This measure could be improved if more steering is used to counteract the yaw moment created by the uneven braking, allowing more brake force to be applied.

The vehicle used in this test is the tractor-semitrailer combination and the setup follows the recommendations of the Swedish ISO Standard, [26]. The friction coefficient on the left side is varied between 0.1 and 0.3, which is considered low, e.g. like an icy surface. The friction coefficient on the right side is high at 1, which could correspond to dry asphalt. The vehicle is traveling with a initial speed of 80 km/h before the brakes are applied. To be able to counteract the moment created by the uneven braking, steering is used on the steerable axles. In the ISO Standard it is stated that the steering wheel angle, connected to the front axle, should not exceed 120° during the maneuver. The deceleration for the braking will be restricted to keep the steering wheel angle under this value.

4.1.2 Single lane change

At high speed an open-loop single lane change maneuver is carried out. The vehicle is first driving at a constant speed and after some time the vehicle is provided with a single-period sinusoidal steering input at the front axle.

There are several important performance characteristics that can be evaluated from this test scenario. One characteristic studied is the rearward amplification (RWA), which highlights the yaw stabilization at high speed. During a lateral movement each unit in the combination experiences different lateral accelerations which amplifies backwards.

RWA in this thesis is defined as, [23]: *"The ratio of the maximum yaw rate of the vehicle frame following vehicle unit to that of the first vehicle unit during a specified maneuver at a certain friction level and constant speed"*.

RWA could also be defined in terms of lateral accelerations, but since yaw rate is a global variable, i.e. each unit has the same yaw rate, it is more reliable according to [1]. A high value of RWA indicates that there is a risk of hitting objects on the sides or causing the rear units to rollover. A RWA-value of 1 is optimal, and it is therefore desired to have a control system that can achieve this.

Another important property to consider, regarding stability and handling of longer combinations, is how fast yaw oscillations of articulation joints is stabilized after a maneuver. One measure to study this, is the yaw damping coefficient (YDC). If there is not much damping of the oscillations, the driver workload and the safety risk might be increased.

YDC is defined as, [23]: *"The damping ratio of the least damped articulation joint's angle of the vehicle combination during free oscillations excited by actuating the steering wheel with a certain pulse or a certain sine-wave steer input at a certain friction level."*

The damping ratio is calculated via the logarithmic decrement, which is defined for an under-damped system and the procedure is described in [25]. A damping ratio close to 0 is a very badly damped system, whereas a system with a ratio close to 1 have a very good damping.

The single lane change maneuver is performed on the A-double combination and follows the recommendations of the Swedish ISO Standard, [24]. The start speed is 80 km/h and amplitude and frequency of the sine-wave steer input is set according to

$$\begin{aligned} \delta_{11} &= Asin(2\pi ft) \\ A = 0.03 \text{ radians and } f &= 0.31 \text{ Hz} \end{aligned} \tag{4.1}$$

The amplitude is chosen to not exceed the recommended maximum lateral acceleration of 2 m/s^2 of the first unit during the maneuver. The frequency is chosen to achieve the greatest RWA-value during the lane change, and this value could be concluded after test simulations for different frequencies. RWA-values for the uncontrolled A-double as a function of the frequency of the steer input, together with corresponding maximum yaw rates, is shown in Figure 4.1. At the moment the steer action is provided, the accelerator pedal is released.

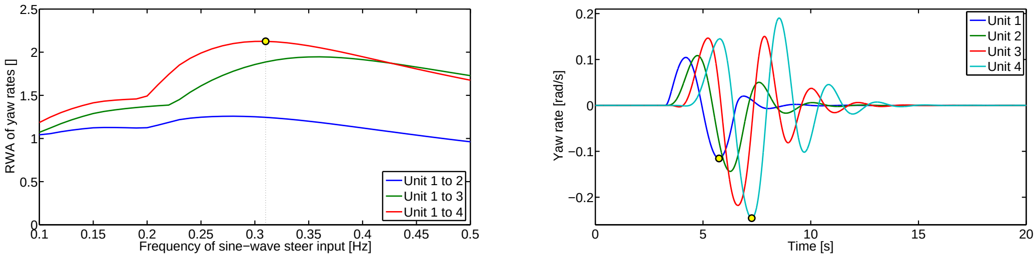

Figure 4.1: Single lane change maneuver for the uncontrolled A-double combination. Left: RWA-values for different frequencies of sinusoidal steer input. Right: Corresponding yaw rates at the frequency where the RWA-value is maximum, marked as yellow dots.

4.1.3 180 ° turn

At low speed, a 180 ° turn is performed, this corresponds to turning back through a roundabout. The test is carried out in closed loop to guarantee the predefined path.

A relevant performance measure for this maneuver is the low speed steady-state off-tracking. During a turn in low speed the path of the rear wheels is going inside the path of the front wheels which will require more space for the combination compared to when going straight.

Low speed steady-state off-tracking is defined as: *"The lateral offset between the paths of the center of the front axle and the center of the most severely off-tracking axle of any unit in a steady turn at a certain friction level and a certain constant longitudinal speed."*

The Directive 96/53 EG, [27], is the base for the test. The vehicle is from the beginning traveling at a constant speed of 5 km/h and is driving straight in approximately 10 meters. It then performs a 180° left turn at a radius of 12.5 meters at the outermost point of the combination, which is the point at the right front of the first unit. The friction coefficient is always kept constant at 1 during the maneuver. If the combination have steering on other wheels than at the front axle, there is a possibility to decrease the off-tracking by steering on the rear wheels.

4.2 Simulation results

How the B-matrix is used, different control strategies, and the simulation results for each test scenario, are presented in the following sections. The simulations are carried out using *Simulink* and Volvo's *Virtual Truck Model* (VTM) library [12]. The model parameters for the simulations can be found in Appendix A.3.

The different variants of control input vectors are presented in Appendix A.1. The maximum number of actuators for the test vehicles is 31 actuators for the full A-double combination. In this thesis there is no need to optimize the execution time in the solvers and the active set method is used as the optimization solver for all simulation setups.

4.2.1 Choice of B-matrix

In section 3.3 three different B-matrices are derived. These are tested in simulations and a study of the structures is also made. Despite the easier structure of the Newton-matrices, the treatment of articulation angles in the Lagrange-matrix describes the real behavior of the vehicle better. Therefore, the B-matrix in (3.31) is the only one kept for further simulations.

For the two test vehicles, the tractor-semitrailer and the A-double combination, the virtual control vectors are

$$\begin{cases} v_{TS} = (F_{X_1}\ F_{Y_1}\ M_{Z_1}\ M_{\theta_1})^\intercal \\ v_{A-dobule} = (F_{X_1}\ F_{Y_1}\ M_{Z_1}\ M_{\theta_1}\ M_{\theta_2}\ M_{\theta_3})^\intercal \end{cases} \tag{4.2}$$

At high speed, the steer and articulation angles will in general be small. Under high speed maneuvers there is also a possibility to apply maximum brake force. As explained in section 2.1, the longitudinal forces will then dominate, meaning that lateral forces will be lost if a high brake force is applied. An appropriate simplification is then to set the terms $sin(\cdot)$ and $cos(\cdot)$ to 0 and 1, respectively. This simplification is used in the two high speed simulations, the single lane change and split friction maneuver. In the low speed 180° turn, the structure of the original matrix is used, with some small changes. To be able to use the feed-forward function explained in section 3.3.1, the terms in the B-matrix related to the steer actuators must be approximated to only generate lateral forces and moments. The approximation implies that no consideration will be taken to the negative forces generated via large steer angles. This phenomena could for example be compensated for using a speed controller.

The original B-matrix in (3.31) for the full A-double combination, without any simplification of small angles are presented in Appendix A.2.

4.2.2 Split friction braking

The split friction maneuver is performed on four different configurations of the tractor-semitrailer, where three of them uses control allocation for the vehicle control. It is assumed that the friction level is estimated in some way and therefore known to the allocator. The tested configurations are as follows.

- *Vehicle 1 - Reference vehicle without control allocation.* The controlled actuators are the front steer angle and brake torques on each wheel. The control strategy for the second unit is to take maximum brake force that can be achieved on the low friction side and use the same on the high friction side, which will eliminate the risk of sliding out with the second unit. On the first unit, the strategy is to use maximum brake force on the low friction side and apply more brake force on the high friction side until counter-steering by 120° on the steering wheel angle is reached.
- *Vehicle 2 - Vehicle equipped with control allocation.* The controlled actuators are the front steer angle and brake torques on each wheel. For the control input vector corresponding to this vehicle, see (A.1).
- *Vehicle 3 - Vehicle equipped with control allocation.* The actuators controlled are the front steer angle, steer angles on the second unit and brake torques on each wheel. For the control input vector corresponding to this vehicle, see (A.2).
- *Vehicle 4 - Vehicle equipped with control allocation.* The actuators controlled are the front steer angle, steer angles on the second unit and brake torques on each wheel. The steer angles on the second unit are restricted to all be same. For the control input vector corresponding to this vehicle, see (A.2).

These vehicle configurations are referred to as Vehicle 1 ... Vehicle 4 in the following.

Control strategy

In this braking maneuver the longitudinal forces are in focus. The generation of the target for F_{X_1} is done with a speed controller according to

$$F_{X_1} = \overline{M} a_x \tag{4.3}$$

where $\overline{M}$ is total mass of the combination and a_x is the desired acceleration. The maximum possible brake force is the target, which correspond to $a_x = -0.7g$, where g is the gravitational constant.

The targets for F_{Y_1} and M_{Z_1} are generated via feed-forward of the steer angle provided from a driver model in feedback according to Figure 3.1. This driver model is set to keep a straight path during the maneuver. The uneven braking gives a yaw moment which the driver wants to counteract by turning the steering wheel, generating a steer angle at the front axle. This steer angle gives the targets for F_{Y_1} and M_{Z_1} to in total get a vehicle with zero yaw moment.

It is important to meet the regulation requirements of maximum steering wheel angle and the same procedure as described for the reference vehicle is used. This means that the brake force is restricted to still achieve 120° on the steering wheel. This maneuver can be considered as a critical situation and angle overlay is used to help the driver. The allowed angle overlay is varied between $\pm 1, 2, \ldots 10°$.

The target for the second unit is to achieve $M_\theta = 0$, i.e. it is desired to keep a straight path. The allocator is then let to decide the steering angles needed to achieve this target.

The weighting matrix for the virtual control signals, W_v, is set to prioritize in the following order. F_{X_1} is most important to satisfy, moments on all units is second most important and lowest priority is set to F_{Y_1}. The W_v-matrix used, corresponding to this priority, is

$$W_v = \begin{pmatrix} 10 & 0 & 0 & 0 \\ 0 & 0.1 & 0 & 0 \\ 0 & 0 & 1 & 0 \\ 0 & 0 & 0 & 1 \end{pmatrix} \tag{4.4}$$

The front steer angle have the restriction to the maximum steering wheel angle (120°), together with $\pm$ the angle overlay, and the total angle is not allowed to exceed $\pm 45°$. This is used in u_{min} and u_{max}. The limitations of torque actuators uses the friction ellipse (2.6) to set appropriate maximum and minimum values, i.e. $\pm \mu F_z$. Due to this simple model there is no consideration into how large the longitudinal slip is. A problem that can arise during a hard brake-in, if the slip is to high, is that the wheels lock. This corresponds to going to the right after the peak in the force-slip curve Figure 2.4, where the tire forces are lost. To avoid this problem a simple ABS-function is used to restrict the longitudinal slip to stay under a certain slip level. The ABS-function is used before the actuator signals are sent to the vehicle motion system.

The tuning parameters W_u and u_{des} can be chosen to make the allocator choose actuators in a desired way. The W_u-matrix tells how to prioritize which actuators that is most important to achieve the desired usage in u_{des}. In general for all maneuvers, the steering actuators is prioritized to be used before brakes and driving, due to energy minimization. In the W_u-matrix, which has the same diagonal form as W_v, the steering actuators is set with to the weighting 1. The torque actuators is set relative to the their normal forces, presented in [5], according to

$$W_{u,trq} = \sqrt{mg}\ \mathrm{diag}\left(\frac{1}{\sqrt{F_{z11l}}}\ \frac{1}{\sqrt{F_{z11r}}} \cdots \frac{1}{\sqrt{F_{zn_un_{anu}l}}}\ \frac{1}{\sqrt{F_{zn_un_{anu}r}}} \right) \tag{4.5}$$

where the terms $\frac{1}{\sqrt{F_z}}$ are limited to be at maximum 100. Under normal conditions, these weighting factors are approximately in the magnitude of 2-4. To impel the allocator to find the desired actuator usage, the parameters in u_{des} is set accordingly. The desired usage for the front steer angle is the angle generated from the driver model. For the second unit's steer actuators, there are no predefined steer angles. The allocator is left to choose these and the terms in u_{des} are set to zero. The wheel torques are desired to be used as little as possible and are therefore set to zero.

For this test case, the tuning parameter γ is set to 0.01, which gives good numerical stability. Due to the inner relative dimension, as mentioned in section 3, this weighting in the optimization problem gives a proper relation between the two terms. This magnitude of γ is also recommended by [16].

Results

As can be seen in Table 4.1, when comparing the stopping distance between Vehicle 1 and Vehicle 2, it is clear that equipping a vehicle with control allocation decreases the stopping distance. If the actuators are weighted as described in equation (4.5) the allocator chooses to apply brake torques in a more optimal way, which results in a higher braking force. This leads to a improved stopping distance compared to Vehicle 1.

Table 4.1: Stopping distances, $\mu = 0.1$

Vehicle configuration	**Stopping distance [m]**
Vehicle 1	87.39
Vehicle 2	83.42
Vehicle 3	86.60
Vehicle 4	72.95

By adding steering to the second unit, the stopping distance is improved compared to Vehicle 1. In that case, the allocator is allowed to brake more unevenly on the second unit since the steer actuators can counteract the moment that is generated. It could be expected that Vehicle 3 and Vehicle 4 behaves similar but Table 4.1 shows a clear difference in the stopping distance. The origin of the difference have not been investigated further.

The drawback of Vehicle 2 can be seen in Figure 4.2, the errors in the allocation are quite large which may cause a undesired behavior of the vehicle.

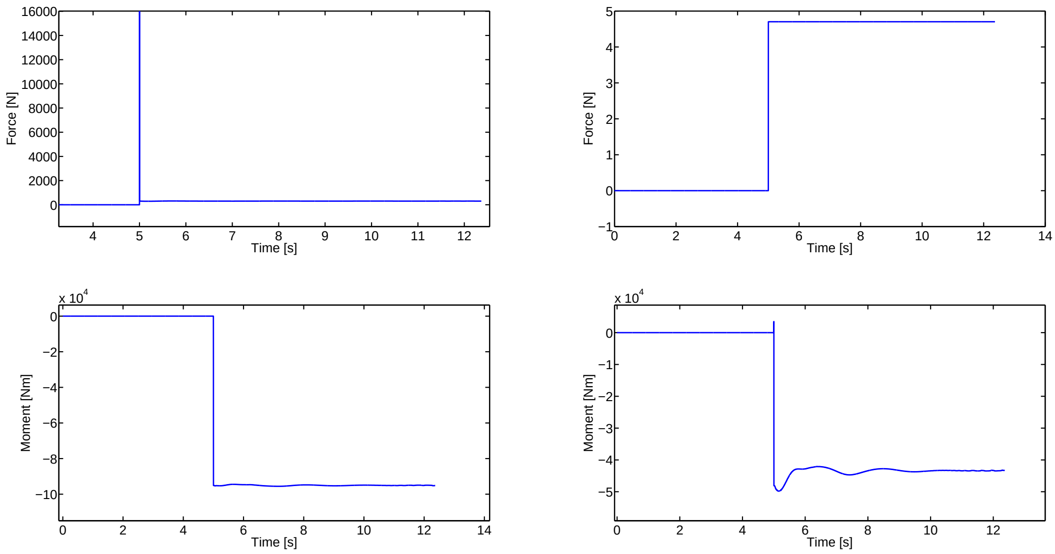

Figure 4.2: Mapping error $Bu - v$ for Vehicle 2, $\mu = 0.1$. Upper left: Error in F_{X_1} (zoomed for clarification). Upper right: Error in F_{Y_1}. Lower left: Error in M_{Z_1}. Lower right: Error in M_{θ_1}.

The moment errors are especially large and these can be explained by the uneven braking. The reference for M_θ is set to zero and this means that the allocator strives for braking equal on both sides of the second unit to not generate a moment in the articulation joint. By weighting F_{X_1} high, the allocator is forced to choose a solution where the vehicle brakes unevenly and a large error in M_θ is to be expected. This means that a moment is generated in the articulation point and should cause an articulation rate. Even though the errors are large, the articulation rate is small, which have two reasons. The main reason is explained by the ratio between the track width t and the wheel base wb. For a long unit, such as the semitrailer, the ratio $\frac{t}{wb}$ is small, and by applying an uneven braking on the two sides of an axle, the lateral motion generated at the axle is small. Due to this geometry, the motion of the second unit is not that large even if the error is. The other reason could be explained by the ABS-function, which limits the slip. The longitudinal forces are applied in such a way that there are always lateral forces left to counteract the moment, and hence prevent the articulation rate.

The large error in M_{Z_1} is due to the feed-forward function, which calculates a moment such that a specific steer angle is chosen by the control allocator. The feed-forward function does not take the uneven braking and created moment into consideration. Therefore, there is an error in M_{Z_1}, which is to be expected.

In Figure 4.3 the mapping errors for Vehicle 3 are shown. This vehicle also have steering on the second unit, and the errors are significantly lower compared to Vehicle 2 with the errors shown in Figure 4.2.

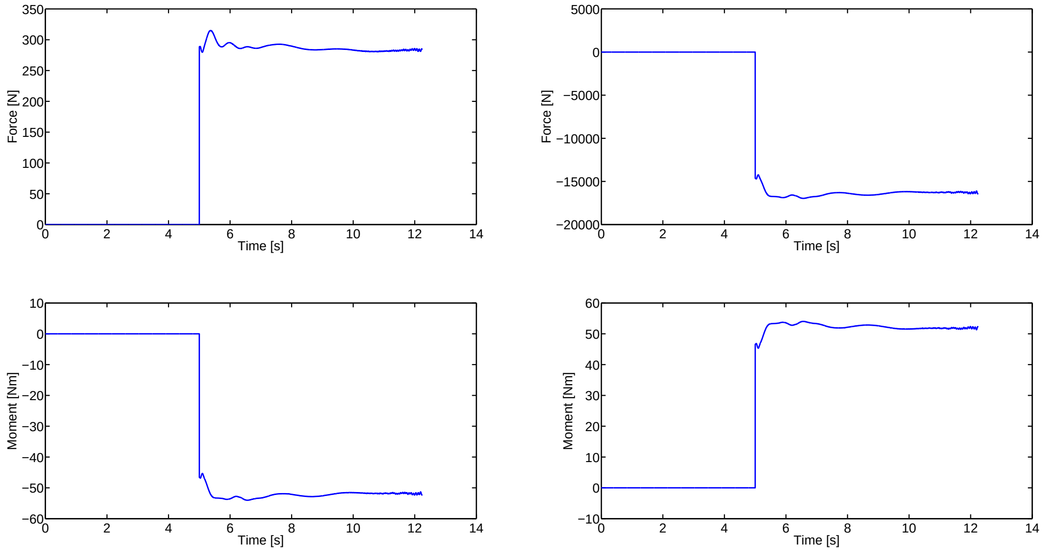

Figure 4.3: Mapping error $Bu - v$ for Vehicle 3, $\mu = 0.1$. Upper left: Error in F_{X_1}. Upper right: Error in F_{Y_1}. Lower left: Error in M_{Z_1}. Lower right: Error in M_{θ_1}.

In Figure 4.4 the second unit's steer actuators, for Vehicle 3, are shown. It is seen that the steer angles are opposite to each other.

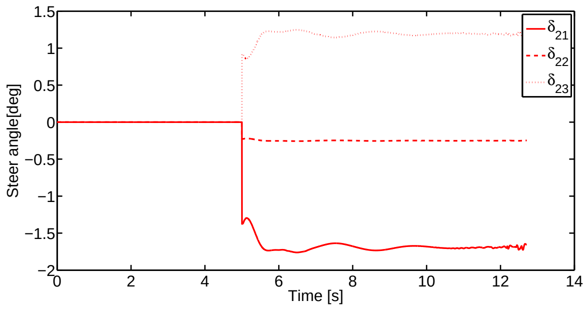

Figure 4.4: The steer angles on the second unit for Vehicle 3.

Steering this way is not desirable and to make the second unit steer in the same direction, the steer actuators are forced to have the same value. This is change done to get Vehicle 4.

In Table 4.2 it can be seen that the vehicle with the shortest stopping distance has the largest deceleration, which is an expected result.

Table 4.2: Average deceleration, $\mu = 0.1$

Vehicle configuration	**Average deceleration** $[\frac{m}{s^2}]$
Vehicle 1	-1.78
Vehicle 2	-1.82
Vehicle 3	-1.78
Vehicle 4	-1.98

The lateral offset from the desired path are shown in Table 4.3. As can be seen from the table, the vehicles equipped with control allocation all have a similar lateral offset. Hence, this measure will not be important when comparing the different vehicles.

Table 4.3: Maximum lateral offset, $\mu = 0.1$

Vehicle configuration	**Lateral offset** $[m]$
Vehicle 1	0.0717
Vehicle 2	-0.1284
Vehicle 3	-0.13
Vehicle 4	-0.1282

In Figure 4.5, the actuator signals for Vehicle 4 is shown. As can be seen from the figure the vehicle applies significantly more brake force on the high friction side. Since the cornering stiffness is high and the lever is long, the steer angles on the second unit is small. In Appendix A.4 corresponding generated tire forces for Vehicle 4, as a result from the control input, are presented.

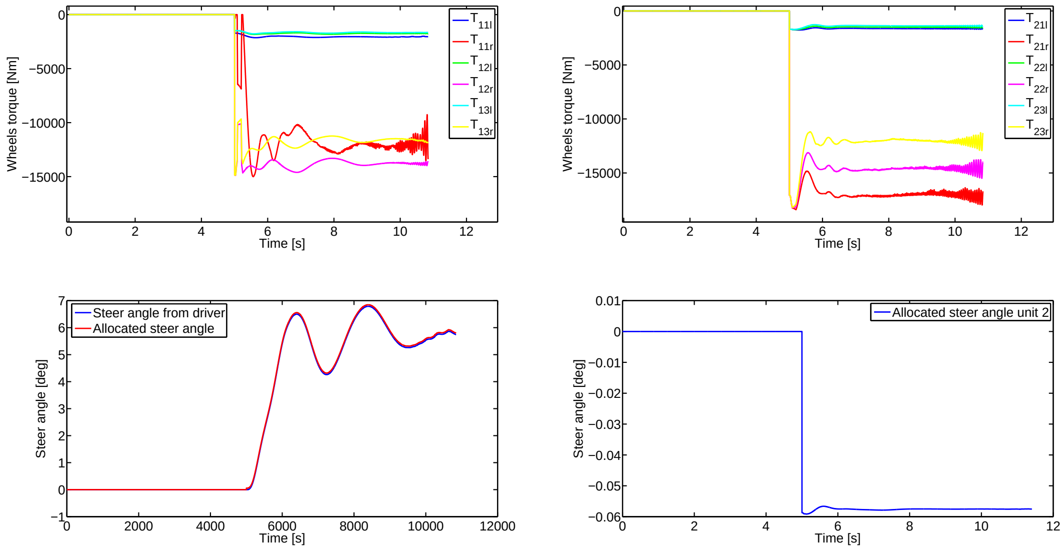

Figure 4.5: Allocated actuator signals for Vehicle 4, $\mu = 0.1$. Upper left: Wheel torques - Unit 1. Upper right: Wheel torques - Unit 2. Lower left: Steer angle unit 1. Lower right: Steer angle unit 2

Parameter study

Angle overlay can be seen as a safety function which overrides the driver input if it is determined to be necessary. For angle overlay it means that the allocator can apply more steer angle than the driver requests. This can be beneficial in a situation where the driver does not react fast enough. The control system can then override the driver and apply control signals that are not requested but determined to be needed for better control of the vehicle. The purpose of angle overlay is that if a larger steer angle is applied more brake force can be applied.

To implement this function, the allocator is allowed to choose a steer angle in a interval around the steer input from the driver. To evaluate the effect of angle overlay in a split friction maneuver, the interval around the steer input is varied between $\pm 1°, 2°, \ldots, 10°$. Vehicle 2 is decelerated with a deceleration that corresponded to 120° on the steering wheel. The friction is varied between $0.1, 0.2$ and 0.3. For $\mu = 0.3$, the driver does not reach 120°, before the brakes are saturated. An example of how angle overlay works is seen in Figure 4.6. The figure depicts a case where the allocator is allowed an angle overlay of 2°. The allocator uses this to steer more than the driver requests because it leads to a more optimal behavior of the vehicle.

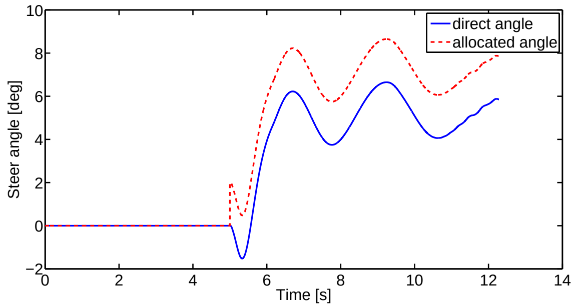

Figure 4.6: The steer angle from the driver and the steer angle from the control allocator.

In figure Figure 4.7 the stopping distance is plotted against the angle overlay. As can be seen from the figure the implementation of angle overlay improves of the stopping distance.

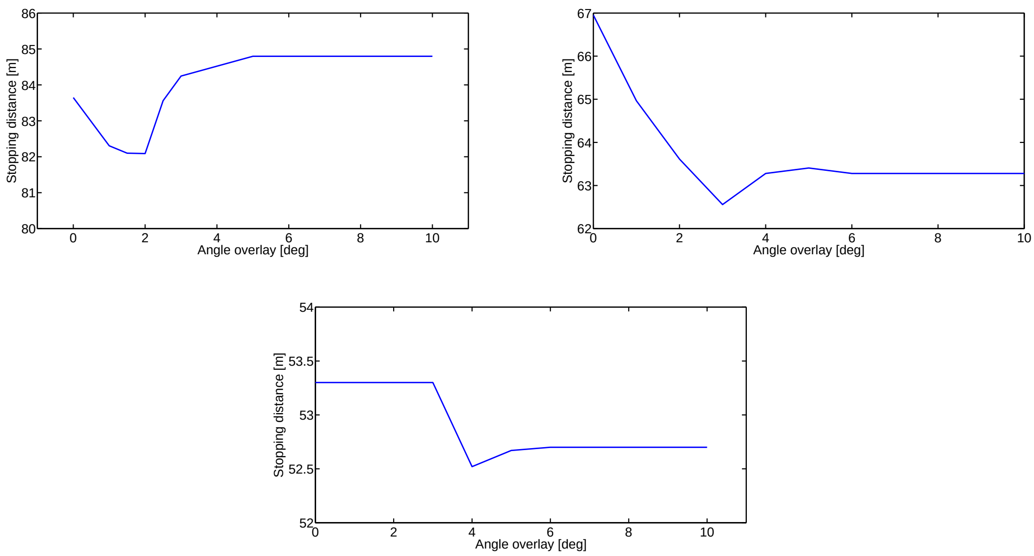

Figure 4.7: Upper left: Stopping distance for $\mu = 0.1$. Upper right: Stopping distance for $\mu = 0.2$. Lower: Stopping distance for $\mu = 0.3$.

For each μ there is a angle that gives a minimal stopping distance, which is 2, 3 and 4° respectively. After these angles there are no further improvement of the stopping distance.

4.2.3 Single lane change

The open-loop single lane change maneuver is performed on five different configurations of the A-double combination, where four of them are controlled. The input steer angle is set according to (4.1). The tested vehicle configurations are as follows.

- *Vehicle 1 - Reference vehicle without control allocation.* The input steer action is applied directly to the front axle and wheel torques are disabled.
- *Vehicle 2 - Vehicle equipped with control allocation.* The input steer action is applied directly to the front axle. Actuators controlled are individual wheel torques, both positive and negative. To generate positive torque, electric machines are used and to produce negative torques, pneumatic brakes are used. For the control input vector corresponding to this vehicle, see (A.3).
- *Vehicle 3 - Vehicle equipped with control allocation.* The input steer action is applied directly to the front axle. Actuators controlled are individual wheel torques, positive and negative, which are both generated from electric machines. This setup is referred to as torque vectoring and could save energy, due to the absence of pneumatic brakes and the possibility to use regenerative braking. For the control input vector corresponding to this vehicle, see (A.3), where all torques are restricted to zero.
- *Vehicle 4 - Vehicle equipped with control allocation.* The input steer action is applied directly to the front axle. Actuators controlled are all steer angles on the following units. No wheel torques are used to control the motion. For the control input vector corresponding to this vehicle, see (A.4).
- *Vehicle 5 - Vehicle equipped with control allocation.* The input steer action is applied directly to the front axle. The actuators controlled are all steer angles on the following units and individual wheel torques on the whole combination. To generate positive and negative wheel torque, electric machines and pneumatic brakes are used respectively. For the control input vector corresponding to this vehicle, see (A.4).

These vehicle configurations are referred to as Vehicle 1 ... Vehicle 5 in the following.

Control strategy

In this maneuver it is important to improve the RWA- and the YDC-parameters. The target is to get closer to 1 in both RWA and YDC compared to the reference vehicle. If the yaw rate of all units followed the first unit's yaw rate, but time delayed, this would be achieved.

According to the test scenario setup in section 4.1.2, the accelerator pedal is released during the maneuver. But in some of the vehicle configurations there are electrical engines at the wheels which could generate positive torque. In those cases there is a possibility to try keeping the speed during the maneuver. A speed controller to generate a reference in F_{X_1} is set according to

$$F_{X_1} = K_x \overline{M}(v_{x0} - v_{x1}) \tag{4.6}$$

where $\overline{M}$ is the total mass of the combination, v_{x0} is the initial speed set to 80 km/h, v_{x1} is the measured speed of the first unit and K_x is a proportional gain used for tuning. After tuning, the parameter K_x is set to 2.

When the input steer angle is given and applied in open loop, there is no need to send this signal through the control allocator. The steer angle is in this maneuver instead provided directly to the vehicle and the allocator focused on forcing the following units to follow a given target of the movement. To incorporate this, the virtual forces for F_{Y_1} and M_{Z_1} are set to 0 and given low priority in W_v.

Targets for the moment in the articulations of the following units are calculated via a simple feedback controller. This is based on a proportional gain, and a delayed yaw rate from the first unit to mimic the movement of the first unit. For example, the virtual moment in the first articulation is set according to

$$M_{\theta_1} = K_{\theta_1}(J_2 + J_3 + J_4)\dot{\theta}_{1,error} = K_{\theta_1}(J_2 + J_3 + J_4)(\dot{\theta}_{1,ref} - \dot{\theta}_{1,meas})$$

$$\begin{cases} \dot{\theta}_{1,ref} = (\omega_{z2,delay} - \omega_{z1,meas}) \\ \dot{\theta}_{1,meas} = (\omega_{z2,meas} - \omega_{z1,meas}) \end{cases} \implies$$

$$M_{\theta_1} = K_{\theta_1}(J_2 + J_3 + J_4)(\omega_{z2,delay} - \omega_{z2,meas}) \tag{4.7}$$

where K_{θ_1} is a proportional gain used for tuning, J_j is the yaw moment of inertia for unit j, $\omega_{z2,meas}$ is the measured yaw rate of the second unit and $\omega_{z2,delay}$ is the reference yaw rate of the second unit, defined as the first units yaw rate but delayed in time. Notice the use of the yaw rate difference $\omega_{z2} - \omega_{z1}$, which is the articulation rate $\dot{\theta}_1$. The inertias used in the equations are the inertias behind the given articulation. For instance, for the last articulation only the inertia of the last unit is used. This seems like the most reasonable choice to describe the articulation moment, and shows satisfying result. After tuning, the gains for the controller are set to 40, 55 and 45 for K_{θ_1}, K_{θ_2} and K_{θ_3} respectively. The time delays, to delay the yaw rates, are calculated as the distance between the units' CoG divided by the initial speed, approximated to be constant.

As mentioned above, it is important for the following units to follow the yaw rate of the first unit, and if possible keep the speed. This is incorporated to the problem formulation by choosing the diagonal weighting matrix W_v appropriately. The matrix in this test case is set to

$$W_v = \begin{pmatrix} 1 & 0 & 0 & 0 & 0 & 0 \\ 0 & 0.001 & 0 & 0 & 0 & 0 \\ 0 & 0 & 0.001 & 0 & 0 & 0 \\ 0 & 0 & 0 & 5 & 0 & 0 \\ 0 & 0 & 0 & 0 & 5 & 0 \\ 0 & 0 & 0 & 0 & 0 & 5 \end{pmatrix} \tag{4.8}$$

For some of the test vehicles torques on each wheel are used. The limitations for the pneumatic brakes is set according to the friction ellipse (2.6). For generating drive torques during the maneuver, electric machines are used. During high speed, it is not possible to achieve maximum positive torque according to the friction ellipse, this due to the characteristic of a general engine. Instead, the limitation for drive torque is approximated to 10 % of the friction ellipse. For some vehicle configurations, also the brake torques are generated via the electric machine. The limit for these negative torques is also set to 10 % of the friction ellipse, but in negative direction. For the steer actuators there is a limit of approximately $\pm 5\,^\circ$ that can be achieved from them. The steer angles on the following units are also restricted to be the same for each unit.

The controller gains in (4.7) are tuned to improve the performance measures, RWA and YDC. In the cases where only wheel torques are used to control the motion there is a trade-off between keeping the speed and improving the RWA- and YDC-measures. Using more brake torque will work against the speed controller and lower the speed. The tuning of the gains for those vehicles is therefore limited to not let the speed drop below 75 km/h during the maneuver.

Actuator priority in W_u and desired actuator utilization in u_{des} is set in the same way as the in the split friction maneuver. The only difference is that the desired usage of the front steer angle is set according to (4.1).

The tuning parameter γ is set to 0.001 in most of the cases, and when steering is used γ is set to 0.01. This parameter turned out to be important in this test scenario.

Results

The steer input is provided after 3.23 seconds and returned to normal at the time of 6.46 seconds. The measured yaw rates for all units, for every vehicle setup, is shown in Figure 4.8. Corresponding RWA-values and YDC-values are depicted in Table 4.4 and Table 4.5 respectively.

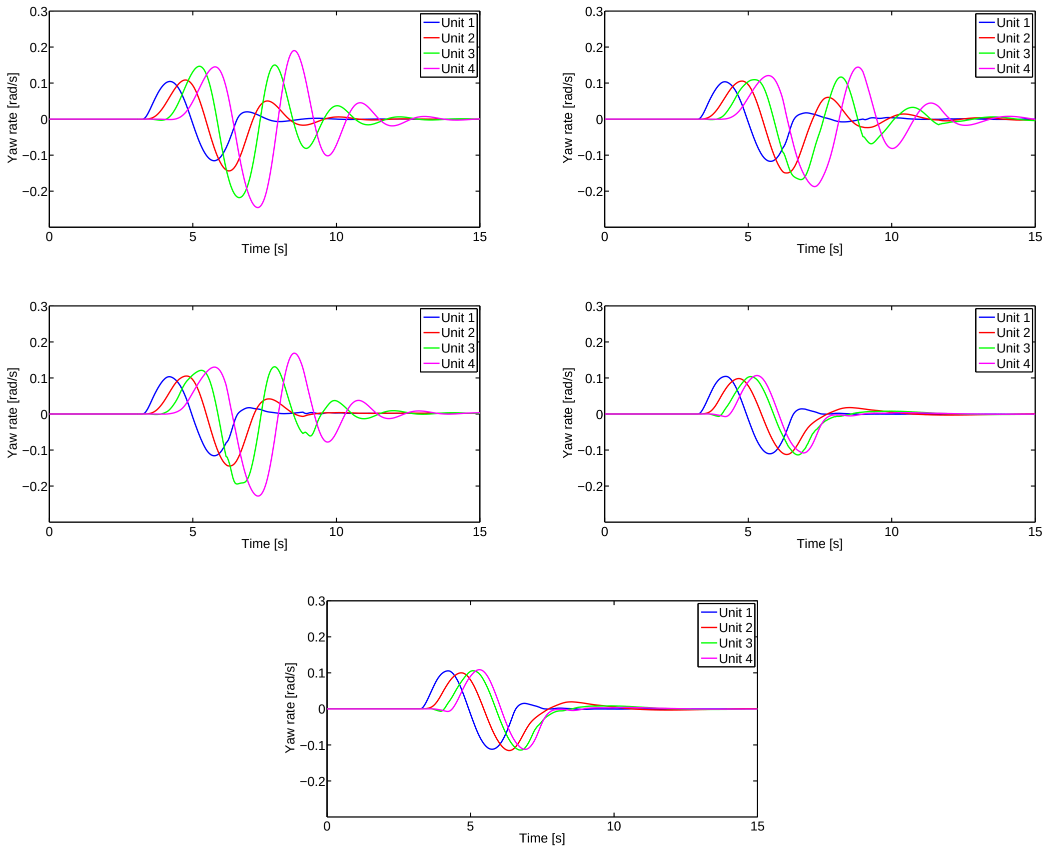

Figure 4.8: Yaw rates for the single lane change maneuver. Upper left: Vehicle 1. Upper right: Vehicle 2. Middle left: Vehicle 3. Middle right: Vehicle 4. Lowest: Vehicle 5.

Table 4.4: RWA-values

Vehicle configuration	**RWA [ ]**
Vehicle 1	2.13 (at unit 4)
Vehicle 2	1.60 (at unit 4)
Vehicle 3	1.97 (at unit 4)
Vehicle 4	1.03 (at unit 3)
Vehicle 5	1.03 (at unit 2)

Table 4.5: YDC-values

Vehicle configuration	**YDC** [ ]
Vehicle 1	0.11 (at articulation 3)
Vehicle 2	0.10 (at articulation 2)
Vehicle 3	0.12 (at articulation 3)
Vehicle 4	0.45 (at articulation 1)
Vehicle 5	0.45 (at articulation 1)

The simulation results show the improvements in the relevant performance measures when introducing more actuators and control allocation to control the motion. In an energy perspective, it is more desirable to use steer actuators compared to wheel torques, and to improve the performance in this maneuver steering is much more efficient.

In all cases when torque actuators is used, the behavior of the vehicle is not as smooth as for the usage of only steer actuators, which is depicted in Figure 4.8 for Vehicle 2. For this vehicle, the RWA-value is improved, compared to Vehicle 1, but the YDC-value is somewhat worse. So, even if the amplification backwards is better, the damping is worse, with a more slightly more nervous behavior of the vehicle.

By only using electric machines to generate both drive and brake torques, as for Vehicle 3, the performance measures are not improved much. Torque actuators needs to generate large control signals to get a moment large enough to stabilize the movement. For Vehicle 3, the torque is restricted to $\pm 10\%$ of the maximum torque available from the friction ellipse, which does not give enough moment to control the motion as desired. The benefits of only using electric machines to improve the performance could be discussed.

In Vehicle 4 and 5, steer actuators are used on both configurations and wheel torques are available on Vehicle 5, but there is no significant difference in the results. For a specific axle, the longitudinal forces generated from torque actuators needs to be larger, compared to the lateral forces generated from steer actuators, to get the same moment. This since the lever is longer for lateral forces, whereas for longitudinal forces the lever is smaller in comparison. The lever difference, and also weighting in W_u between the actuators, will prioritize the usage of the steer actuators when stabilizing the movement. The benefit of adding torque actuators, as in Vehicle 5, is that the speed could be kept better during the maneuver. The allocated wheel torques and steer angles for Vehicle 5 is shown in Figure 4.9.

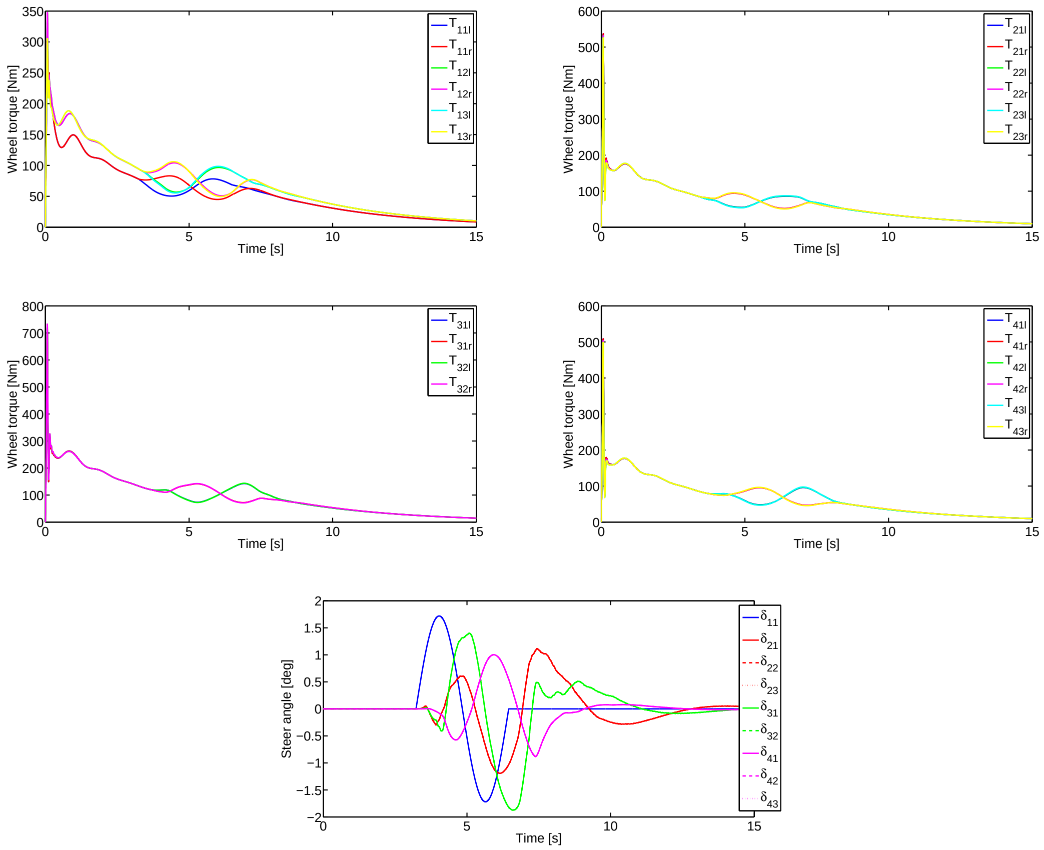

Figure 4.9: Allocated actuator signals for Vehicle 5. Upper left: Wheel torques - Unit 1. Upper right: Wheel torques - Unit 2. Middle left: Wheel torques - Unit 3. Middle right: Wheel torques - Unit 4. Lowest: Steer angles.

In the first time period, before the steer action is requested, some torque is applied to all wheels. This is due to the initialization of the simulation, where there is a small speed reduction and the speed controller works to reduce this error. The actual tire forces generated from Vehicle 5, as a result from the control input, are presented in Appendix A.4.

The mapping error $Bu - v$ for Vehicle 5 is shown in Figure 4.10. The error in the beginning for F_{X_1} corresponds to a initialization error in speed of approximately 2 km/h, which is controlled back during the maneuver. The moment and lateral force of the first unit are not important, due to the fact that the steer input is provided directly to the vehicle. Therefore, these errors are not relevant. The errors in M_θ are considered small, with the meaning that the units are controlled to the desired motion.

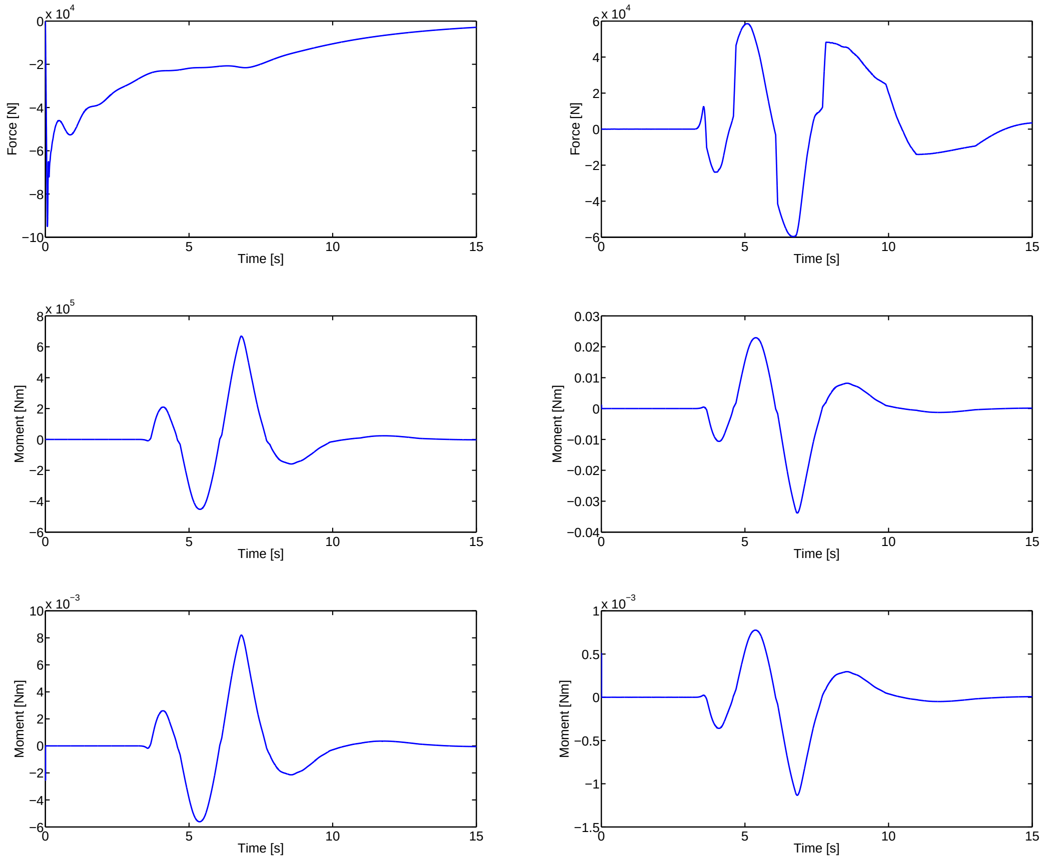

Figure 4.10: Mapping error $Bu - v$ for Vehicle 5. Upper left: Error in F_{X1}. Upper right: Error in F_{Y1}. Middle left: Error in M_{Z1}. Middle right: Error in M_{θ_1}. Lower left: Error in M_{θ_2}. Lower right: Error in M_{θ_3}.

Parameter study

To see how robust the control allocator behavior is, the amplitude of the sine-wave steer input for Vehicle 5 (4.1) is varied. Shown in Figure 4.11 and Figure 4.12 are the allocated actuator signals for the two different amplitudes $A = 0.06$ and $A = 0.09$, respectively. For $A = 0.06$, the behavior is similar as for the initial amplitude in Figure 4.9. As expected, all actuator signals have been increased, mostly for the steer actuators, but the torque actuators as well. For $A = 0.09$, many of the steer angles are saturated to their limits of $\pm 5\,°$. At this point the torque actuators tries to save the situation by applying much larger torques compared to the two previous simulated amplitudes. For this maneuver, with $A = 0.09$, the lateral accelerations are large, just above 10 m/s^2 at the last unit. In general, such large accelerations would result in a roll-over situation, but due to low settings of CoG heights in the VTM-model of for each unit, see Appendix A.3, this phenomenon is not happening. Even for this critical situation, where some actuators are saturated, the RWA-value for the controlled vehicle is 1.62. This can be compared to a simulation of Vehicle 1 for the same amplitude, which gets a RWA-value of 4.37.

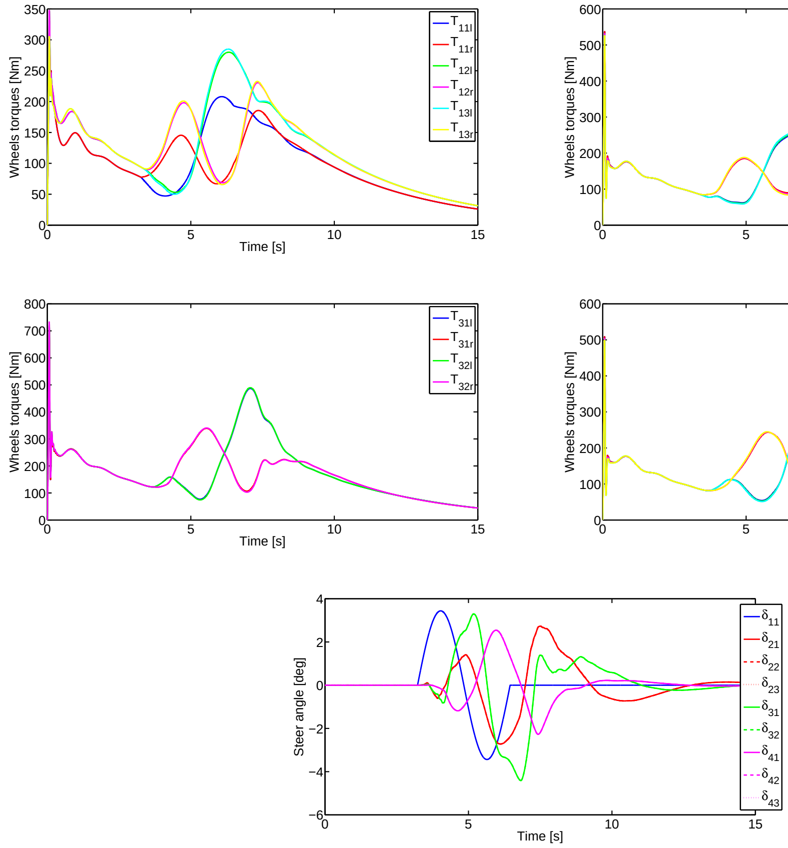

Figure 4.11: Allocated actuator signals for Vehicle 5, A=0.06. Upper left: Wheels torques - Unit 1. Upper right: Wheels torques - Unit 2. Middle left: Wheels torques - Unit 3. Middle right: Wheels torques - Unit 4. Lowest: Steer angles.

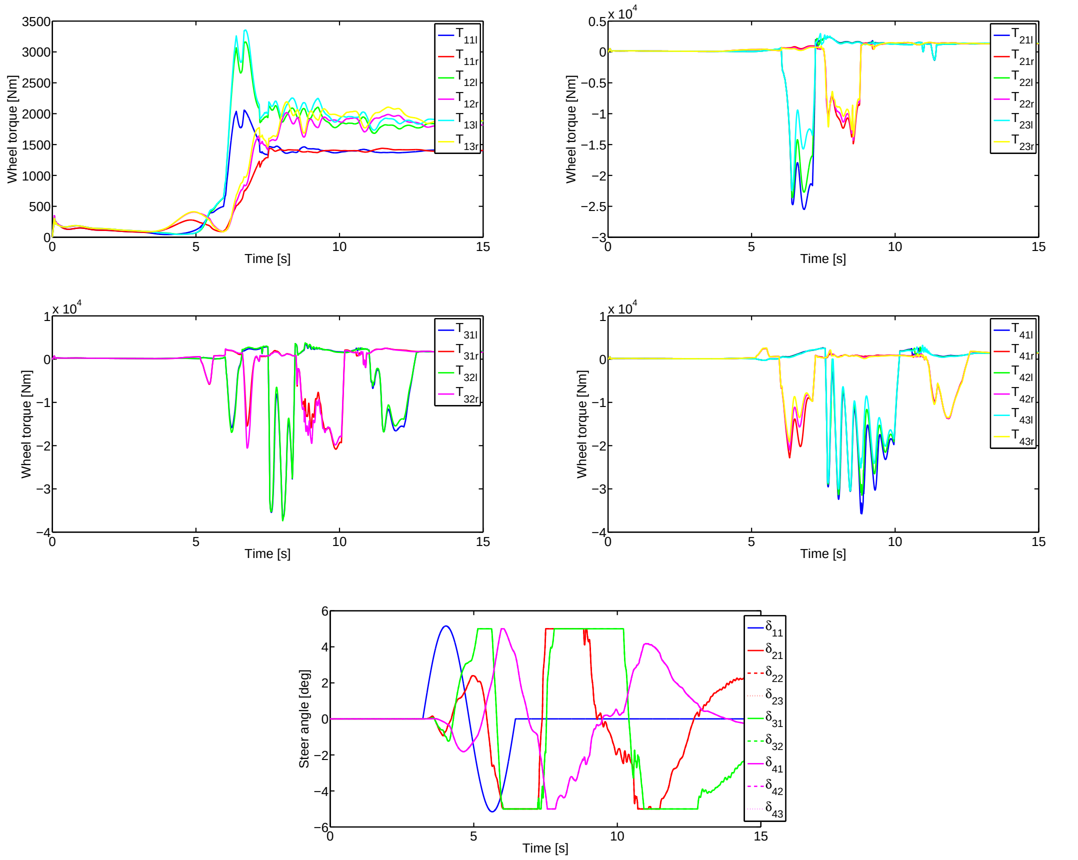

Figure 4.12: Allocated actuator signals for Vehicle 5, A=0.09. Upper left: Wheels torques - Unit 1. Upper right: Wheels torques - Unit 2. Middle left: Wheels torques - Unit 3. Middle right: Wheels torques - Unit 4. Lowest: Steer angles.

4.2.4 180 ° turn

The simulation of the 180 ° turn is performed on three different configurations of the A-double combination, where two of them are controlled with control allocation. The tested vehicle configurations are as follows.

- *Vehicle 1 - Reference vehicle without control allocation.* A driver model generates a steer action at the front axle to follow the specified path. A simple speed controller equally distributes drive torques on the second and third axle of the first unit.
- *Vehicle 2 - Vehicle equipped with control allocation.* Actuators controlled are the front steer angle and following units' steer angles. Drive torques are used on the second and third axle of the first unit.
- *Vehicle 3 - Vehicle equipped with control allocation.* Actuators controlled are the

front steer angle and following units' steer angles. Drive torques on all wheels are also included.

These vehicle configurations are referred to as Vehicle 1 ... Vehicle 3 in the following.

Control strategy

The main objective for this maneuver is to follow a path, where all axles should track the 180° turn as good as possible. During a low-speed turn the speed is reduced and to compensate for this the F_{X_1}-term is generated via a speed controller to keep the initial speed of 5 km/h. The controller have the same form as (4.6) in the single lane change maneuver, and the proportional gain is set to 3.

The targets for the moment and lateral force of the first unit is generated with feed-forward of the front steer angle together with targets for the following units steer angles. The front steer angle is provided via a driver model that tracks the turn with a radius of 12.5 meters at the outermost point of the combination. Generation of targets for steer angles on the following units are based on a very simple control strategy used in [4] for controlling a smart dolly. The technique is extended to be used on the whole combination, not only the dolly (the third unit). The following units' steer angles are set proportional to the front steer angle, and delayed based on the distance from the front axle to the respective axle. This is stated as

$$\begin{aligned} \delta_j &= K_j \delta_{11}(t - t_{delay_j}) \\ t_{delay_j} &= \frac{L_{xj}}{v_x} \end{aligned} \tag{4.9}$$

where K_j is the gain used for tuning, L_{xj} is the longitudinal distance from the front axle to the steered axle on unit j, and v_x is the longitudinal speed, assumed to be constant. The distance L_{xj} will in general vary with the articulation angles, but is approximated to be constant. The longitudinal distance L_{xj} is approximated to the same for all axles on each unit and the setting is 11.10 meter, 16.38 meter and 24.08 meter, for L_{x2}, L_{x3} and L_{x4} respectively. After tuning, the gains are set to -0.85, -0.5 and -0.6, for K_1, K_2 and K_3 respectively. This control strategy is very simple and not optimal, but is enough to see performance improvements when introducing steering on more axles than on the front axle.

When tuning the controller, the requirements are set to make the right side of all axles to track inside the radius of 12.5 meters. In reality, when all axles are steered, the rearmost point of each unit may be running outside. For convenience, this approximation is used to get a estimate of the performance improvements.

It is important to achieve the predefined steer angles, but the speed must also be kept. After tuning, the best weighting among the virtual forces in W_v is set as

$$W_v = \begin{pmatrix} 10 & 0 & 0 & 0 & 0 & 0 \\ 0 & 1 & 0 & 0 & 0 & 0 \\ 0 & 0 & 1 & 0 & 0 & 0 \\ 0 & 0 & 0 & 1 & 0 & 0 \\ 0 & 0 & 0 & 0 & 1 & 0 \\ 0 & 0 & 0 & 0 & 0 & 1 \end{pmatrix} \tag{4.10}$$

The priority among the actuators in W_u are the same as for the previous maneuvers. For the actuator utilization u_{des}, the desired value for the front steer angle is set according to the driver request, and the following units' steer angles are set as the calculated values in (4.9). The desired torque actuator usage is also set the same as before, to zero, to be used as little as possible.

The tuning parameter γ is set to 0.01, to get a stable behavior of the allocator.

Results

In the calculation of steady-state off-tracking, the first axle position is approximated to track a constant radius, as the outermost point of the first unit do. This approximation is considered good enough to see the improvements when introducing more actuators. The maximum off-tracking during the maneuver for the three vehicles compared are presented in Table 4.6. Corresponding trajectories of middle axle positions are shown in Figure 4.13.

Table 4.6: Low speed steady-state off-tracking

Vehicle configuration	**Lateral offset** $[m]$
Vehicle 1	8.08 (at axle 2, unit 4)
Vehicle 2	1.79 (at axle 1, unit 2)
Vehicle 3	1.78 (at axle 1, unit 2)

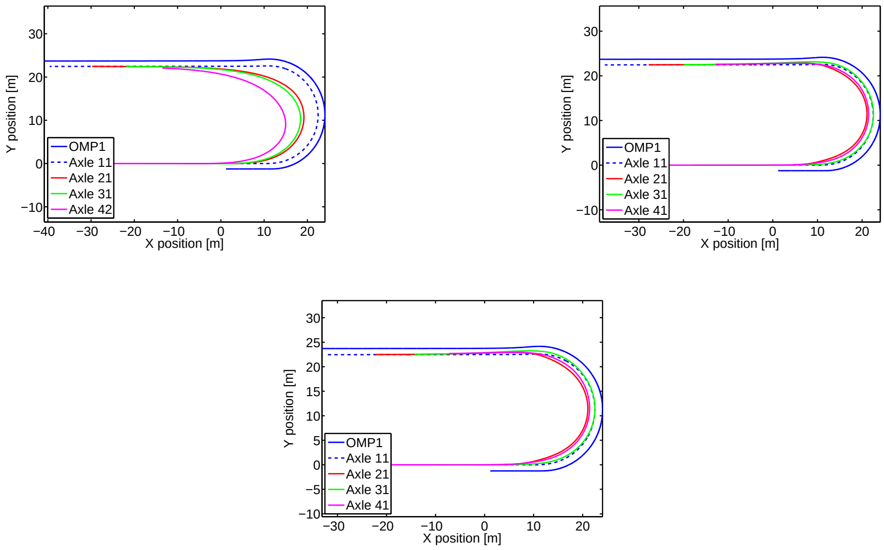

Figure 4.13: Trajectories for middle axle position, together with outermost point on unit 1 (OMP1). Upper left: Vehicle 1. Upper right: Vehicle 2. Lowest: Vehicle 3.

Introducing steer actuators on the following units gives a large reduction in the steady state off-tracking. The difference between Vehicle 2 and 3 is that last configuration uses all wheels for driving the vehicle. This change in vehicle configuration is handled by the control allocator, and the control signals are redistributed to still achieve the same path. The difference in off-tracking between them could be considered negligibly. For Vehicle 3, the allocated signals sent to the vehicle is shown in Figure 4.14.

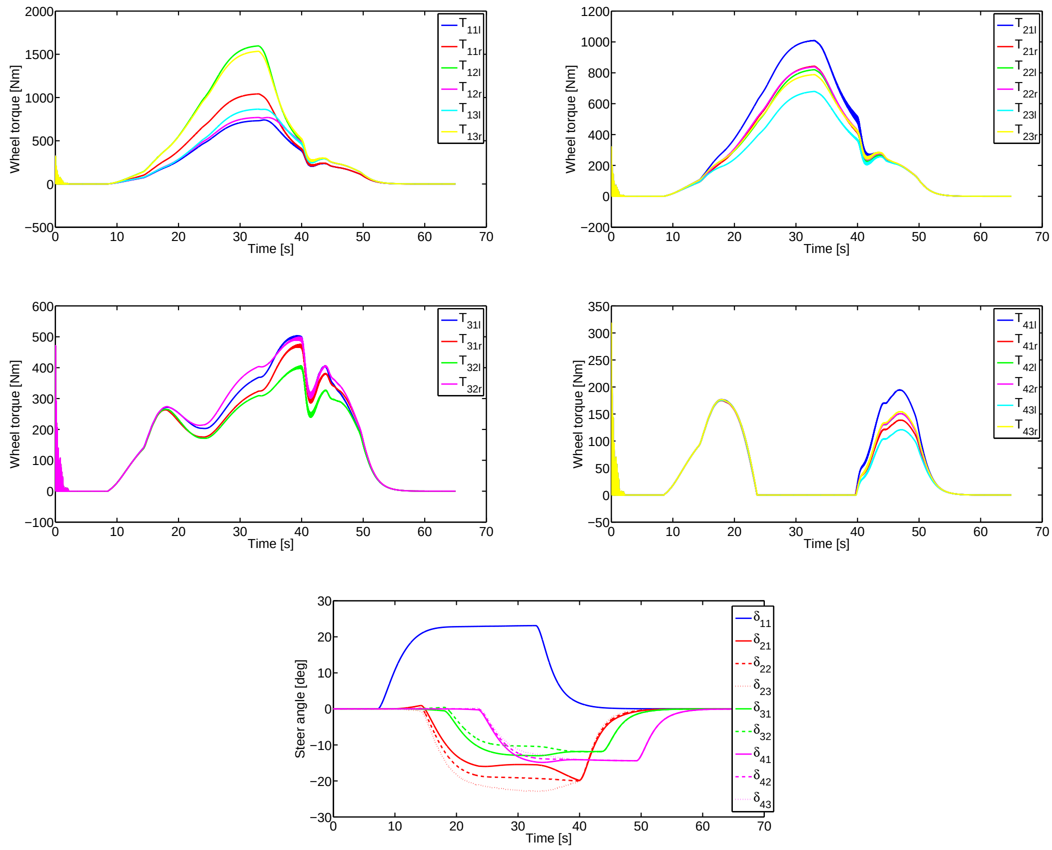

Figure 4.14: Allocated actuator signals for Vehicle 3. Upper left: Wheel torques - Unit 1. Upper right: Wheel torques - Unit 2. Middle left: Wheel torques - Unit 3. Middle right: Wheel torques - Unit 4. Lowest: Steer angles.

The mapping error $Bu-v$ for Vehicle 3 is plotted in Figure 4.15. All errors are very close to zero, expect for the longitudinal force. The F_{X_1}-error corresponds to a reduction in speed from the reference 5 km/h to 4.5 km/h during the turn. The speed is going back to 5 km/h after the maneuver and the error then goes back to zero again. The error is regarded as acceptable during a maneuver like this.

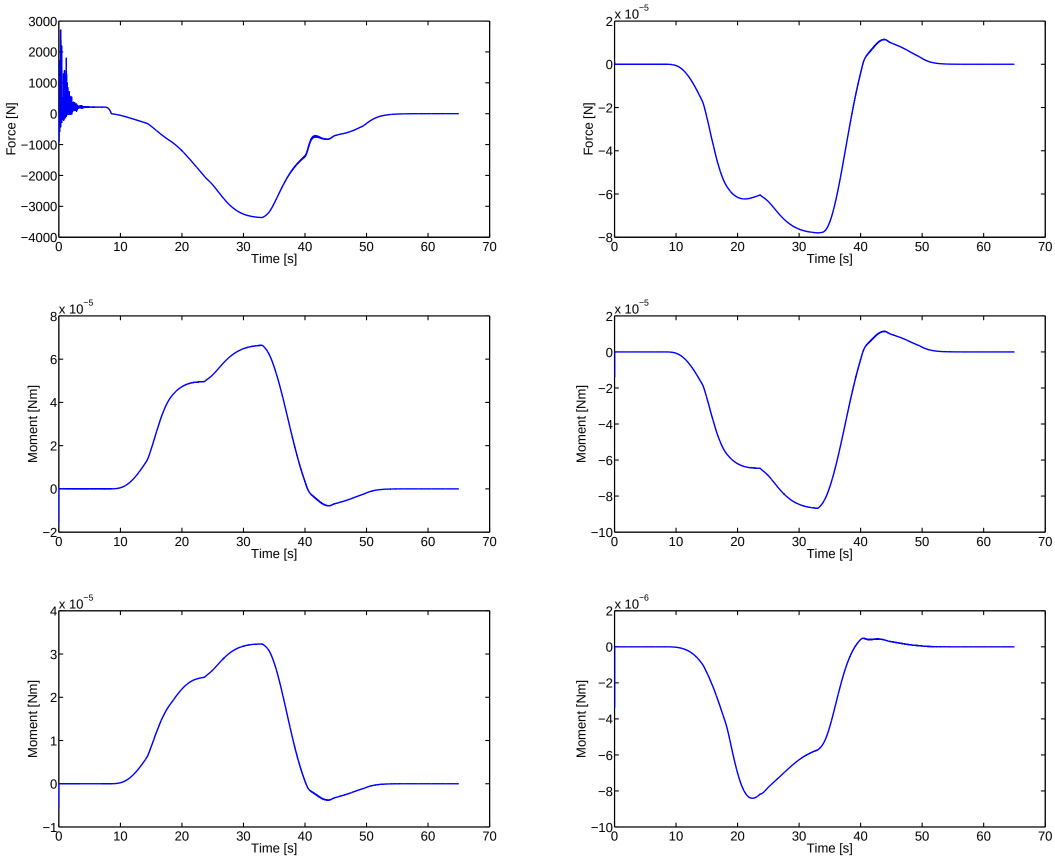

Figure 4.15: Mapping error $Bu - v$ for Vehicle 3. Upper left: Error in F_{X_1}. Upper right: Error in F_{Y_1}. Middle left: Error in M_{Z_1}. Middle right: Error in M_{θ_1}. Lower left: Error in M_{θ_2}. Lower right: Error in M_{θ_3}.

5

Concluding remarks

THE PURPOSE of this thesis, as stated in section 1.2, is achieved. A general control allocation structure for LHV is derived. A vehicle model based on the Lagrange formulation, together with a LPV approximation of the system, was shown to be a satisfactory approach for the control allocation design for LHV. The B-matrix is easily updated in each time step of the simulation with previous measurements of steer and articulation angles.

The B-matrix is derived off-line in a computer algebra tool. It is therefore possible to automatically generate a new B-matrix if another actuator configuration is desired. With the control allocation structure and the computer algebra tool, the change of actuator configuration during simulations has been an effortless procedure, mainly updating the B-matrix. Only with some modifications, the structure could be extended for usage in a arbitrary long heavy vehicle combination.

The proposed control structure is shown to improve the performance in the tested scenarios. The split friction maneuver, performed on the tractor-semitrailer combination, gives a stopping distance of 66.28 meters, compared to the reference vehicle of 87.39 meter. The A-double combination is simulated in a single lane change maneuver and a $180\,^\circ$ turn. The RWA-value in the single lane change is decreased from 2.13 for the reference vehicle, to 1.03. The steady-state off-tracking in the $180\,^\circ$ turn is decreased from 8.08 meters for the reference vehicle, to 1.78 meters. The results show the possibility of using control allocation together with more actuators to get improved performance of a modular vehicle combination. This makes the modular vehicle combination have performance similar to a standard configuration.

5.1 Discussion and future work

The mathematical model in the Newton formulation is based on a coupling model with a spring and damper. An alternative method to model the coupling is to have kinematic constraints relating the velocity and acceleration in the coupling. This could give an alternative state formulation and hence, result in a competitor to the chosen control allocator design.

In the derivation of the B-matrix only planar motion is considered and actuator dynamics are not included. A future study could be to include these into the modeling and see if the performance can be further improved by using a more complex model to derive the B-matrix. Another interesting study would be to keep the problem nonlinear and evaluate if the performance can be improved by using nonlinear optimization.

The linear parameter varying (LPV) B-matrix is used in the low speed maneuver and a simplified version of it in the two other test cases. Early attempts in using the simplified B-matrix in the low speed maneuver shows that it could be questioned if LPV is needed even in the low speed case where large angles are present. Using a static B-matrix is better for a real time implementation. Simulation of other test scenarios are also important, and the best structure of the B-matrix could be further investigated.

The results shows that it is possible to use control allocation for these types of vehicles, but the performance is not optimized. Especially noticed for the single lane change maneuver, there is a sensitivity in the allocator tuning parameters. A more sophisticated evaluation on how both controller and control allocator parameters are affecting the behavior are recommended for future work. Some parameters used in the allocator, such as road friction, are assumed to be known. This is not the real case in reality and a stable and robust estimator is important to include. Many model parameters are also estimated, such as inertias and cornering stiffness, and these can be investigated even more.

In section 4.2.2 it is shown that the stopping distance can be improved by using angle overlay. A future study could be to further explore the mechanisms behind the improvement. If this effect can be explained more specifically, a function can be developed to control the vehicle in a critical situation. This is interesting from a safety perspective.

The configuration of the vehicles, with individual wheel torques and all steerable axles, is not yet applicable in reality, due to cost and complexity. The configurations is used to see how the allocator handles many actuators and the possible performance improvements with that. A more realistic setup to investigate, could be to have drive torque on axle two and three of the first unit, individual wheel brakes and a steerable dolly. In such a case, a comparison between motion control systems used today, and the proposed structure could be made. Implementation in a real truck is also a interesting future step.

In this thesis different control strategies are used for each maneuver. It is desirable to use a standard structure for the controller and one step closer would be to design a controller that works for a large variety of maneuvers. This kind of study would take the control structure closer to a real world implementation.

References

[1] Aurell, J., Wadman, T. (2007) *Vehicle combinations based on the modular concept.* Report no. 1/2007, Committee 54: Vehicles and Transports.

[2] The DUO^2-project in collaboration between companies and agencies. <http://duo2.nu/> (2014-05-02)

[3] Gross Combination Weight. <http://www.irmi.com/online/insurance-glossary/terms/g/gross-combination-weight-gcw.aspx> (2014-05-02)

[4] Sundström, P. (2013) Simulation study on possibilities and actuator requirements for converter dolly with active steering and propulsion. ER-651993. *Volvo Group Trucks Technology.* Confidential.

[5] Tagesson, K., Sundström, P. (2008) *On Real Time Adaptive and Dynamically Constrained Control Allocation for Stability Control of Heavy Vehicles.* Master's Thesis EX081/2008, Chalmers University of Technology, Sweden.

[6] Shyrokau, B., Wang, D. (2012) *Control Allocation with Dynamic Weight Scheduling for Two-task Integrated Vehicle Control.* EXQUISITUS, Centre for E-City, Nanyang Technological University, Singapore.

[7] Yang, X. (2012) Optimal Reconfiguration Control of the Yaw Stability of the Tractor-Semitrailer Vehicle. Hindawi Publishing Corporation, *Mathematical Problems in Engineering*, Volume 2012, Article ID 602502, 23 pages doi:10.1155/2012/602502

[8] Eklöv, J. (2013) *Real-time implementation of a vehicle motion coordinator for a single unit truck.* Master's Thesis EX036/2013, Chalmers University of Technology, Sweden.

[9] Johansen T.A., Fossen, T.I. (2013) Control Allocation - A Survey. *Automatica*, 05/2013, 49(5):1087–1103.

[10] Andersson U. (2013) *Automation and Traction Control of Articulated Vehicles.* PhD Thesis, Luleå University of Technology, Sweden.

[11] An S-i., Kwon D-S. (2011) Zero Moment Point Feedback Balance Control of Leg-Wheel Hybrid Structures by using Dynamic Decoupling and Control Allocation. *IEEE International Conference on Robotics and Automation*, Shanghai International Conference Center May 9-13, 2011, Shanghai, China.

[12] Volvo Truck Model (2014), Simulink library developed at Volvo Group Trucks Technology, Department BF72991.

[13] Sadeghi Kati M. et al. (2013) *Performance Improvement for A-double Combination by introducing a Smart Dolly.* Chalmers University of Technology & Volvo Group Trucks Technology, Sweden.

[14] Jazar, R.N. (2009) *Vehicle Dynamics: Theory and Application.* Springer Science+ Business Media, New York.

[15] Pacejka H. B. (2006) *Tyre and Vehicle Dynamics.* 2nd edition, Butterworth-Heinemann, Oxford.

[16] Nilsson P., Tagesson K. (2013) *Single-track models of an A-double heavy vehicle combination.* Report 2013:08, Vehicle Dynamics Group, Division of Vehicle and Autonomous Systems, Department of Applied Mechanics, Chalmers University of Technology, Sweden.

[17] Chen C., Tomizuka M. (1997) *Modeling and Control of Articulated Vehicles.* California PATH Research Report UCB-ITS-PRR-97-42, University of California, Berkeley.

[18] Jacobsson B. et al. (2013) *Vehicle Dynamics - Compendium for Course MMF062.* Vehicle Dynamics Group, Division of Vehicle and Autonomous Systems, Department of Applied Mechanics, Chalmers University of Technology, Sweden.

[19] Kharazzi S. (2012) *Steering Based Lateral Performance Control of Long Heavy Vehicle Combinations.* PhD Thesis, Chalmers University of Technology, Sweden.

[20] Härkegård O. (2003) *Backstepping and Control Allocation with Applications to Flight Control.* PhD Thesis, Linköping University, Sweden.

[21] Tøndel P., Johansen T. A. (2005) *Control Allocation for Yaw Stabilization in Automotive Vehicles using Multiparametric Nonlinear Programming.* Norwegian University of Science and Technology, Norway.

[22] Bruzelius F. (2004) *Linear Parameter-Varying Systems - an approach to gain scehduling.* PhD Thesis, new series no 2076, report no. 472, Chalmers University of Technology, Sweden.

[23] Sadeghi Kati M. (2013) *Definitions of Performance Based Characteristics for Long Heavy Vehicle Combinations.* Department of Signals and Systems, Chalmers University of Technology, Sweden.

[24] Swedish Standard SS-ISO 14791 (2002) *Road vehicles – Heavy commercial vehicle combinations and articulated buses – Lateral stability test methods.*

[25] ISO 14791. (2002) *Road vehicles — Heavy commercial vehicle combinations and articulated buses — Lateral stability test methods.*

[26] Swedish Standard SS-ISO 16234 (2006) *Heavy vehicles and buses - Straight-ahead braking on surfaces with split coefficient of friction - Open loop test method.*

[27] Council Directive 96/53/EG, *Official Journal of the European Communities*, July 25th 1996, Nr L 235/59.

A

Elucidating material

A.1 Control input vectors

The four variants of vehicles tested and the associated u-vectors:

- Tractor-semitrailer with tractor front axle steerable and individual torques on each wheel.

$$u = (T_{11l}\ T_{11r}\ T_{12l}\ T_{12r}\ T_{13l}\ T_{13r}\ \delta_{11}\ T_{21l}\ T_{21r} T_{22l}\ T_{22r} T_{23l}\ T_{23r})^{\intercal} \tag{A.1}$$

- Tractor-semitrailer with tractor front axle and trailer axles steered, individual torques on each wheel.

$$\begin{aligned} u = (&T_{11l}\ T_{11r}\ T_{12l}\ T_{12r}\ T_{13l}\ T_{13r}\ \delta_{11}\ T_{21l}\ T_{21r} T_{22l}\ T_{22r} T_{23l}\ T_{23r}\ \ldots \\ &\delta_{21}\ \delta_{22}\ \delta_{23})^{\intercal} \end{aligned} \tag{A.2}$$

- A-double with tractor front axle steerable and individual torques on each wheel.

$$\begin{aligned} u = (&T_{11l}\ T_{11r}\ T_{12l}\ T_{12r}\ T_{13l}\ T_{13r}\ \delta_{11}\ T_{21l}\ T_{21r} T_{22l}\ T_{22r} T_{23l}\ T_{23r}\ \ldots \\ &T_{31l}\ T_{31r}\ T_{32l}\ T_{32r}\ T_{41l}\ T_{41r}\ T_{42l}\ T_{42r}\ T_{43l}\ T_{43r})^{\intercal} \end{aligned} \tag{A.3}$$

- A-double with tractor front axle and following units axles steered, individual torques on each wheel.

$$\begin{aligned} u = (&T_{11l}\ T_{11r}\ T_{12l}\ T_{12r}\ T_{13l}\ T_{13r}\ \delta_{11}\ T_{21l}\ T_{21r} T_{22l}\ T_{22r} T_{23l}\ T_{23r}\ \ldots \\ &\delta_{21}\ \delta_{22}\ \delta_{23}\ T_{31l}\ T_{31r}\ T_{32l}\ T_{32r}\ \delta_{31}\ \delta_{32}\ T_{41l}\ T_{41r}\ T_{42l}\ T_{42r}\ T_{43l}\ T_{43r}\ \ldots \\ &\delta_{41}\ \delta_{42}\ \delta_{43})^{\intercal} \end{aligned} \tag{A.4}$$

A.2 Complete B-matrix

The virtual control vector associated to the A-double combination with maximum number of actuators, see (A.4), is

$$v = (F_{X1}\ F_{Y1}\ M_{Z1}\ M_{\theta_1}\ M_{\theta_2}\ M_{\theta_3})^{\intercal}$$

Corresponding B-matrix have the form

$$B = \left(\begin{array}{ccccccc}
\frac{\cos(\delta_{11})}{R} & \frac{\cos(\delta_{11})}{R} & \frac{1}{R} & \frac{1}{R} & \frac{1}{R} & \frac{1}{R} & -2\mathrm{C}\alpha_{11}\sin(\delta_{11}) \\
\frac{\sin(\delta_{11})}{R} & \frac{\sin(\delta_{11})}{R} & 0 & 0 & 0 & 0 & 2\mathrm{C}\alpha_{11}\cos(\delta_{11}) \\
-\frac{t_{11}\cos(\delta_{11})-2l_{11}\sin(\delta_{11})}{2R} & \frac{2l_{11}\sin(\delta_{11})+t_{11}\cos(\delta_{11})}{2R} & -\frac{t_{12}}{2R} & \frac{t_{12}}{2R} & -\frac{t_{13}}{2R} & \frac{t_{13}}{2R} & 2\mathrm{C}\alpha_{11}l_{11}\cos(\delta_{11}) \\
0 & 0 & 0 & 0 & 0 & 0 & 0 \\
0 & 0 & 0 & 0 & 0 & 0 & 0 \\
0 & 0 & 0 & 0 & 0 & 0 & 0
\end{array}\right.$$

$$\begin{array}{cc}
\frac{\cos(\delta_{21}+\theta_1)}{R} & \frac{\cos(\delta_{21}+\theta_1)}{R} \\
\frac{\sin(\delta_{21}+\theta_1)}{R} & \frac{\sin(\delta_{21}+\theta_1)}{R} \\
-\frac{2(a_2+l_{21})\sin(\delta_{21})+2b_1\sin(\delta_{21}+\theta_1)+t_{21}\cos(\delta_{21})}{2R} & \frac{-2(a_2+l_{21})\sin(\delta_{21})-2b_1\sin(\delta_{21}+\theta_1)+t_{21}\cos(\delta_{21})}{2R} \\
-\frac{2(a_2+l_{21})\sin(\delta_{21})+t_{21}\cos(\delta_{21})}{2R} & \frac{t_{21}\cos(\delta_{21})-2(a_2+l_{21})\sin(\delta_{21})}{2R} \\
0 & 0 \\
0 & 0
\end{array}$$

$$\begin{array}{cc}
\frac{\cos(\delta_{22}+\theta_1)}{R} & \frac{\cos(\delta_{22}+\theta_1)}{R} \\
\frac{\sin(\delta_{22}+\theta_1)}{R} & \frac{\sin(\delta_{22}+\theta_1)}{R} \\
-\frac{2(a_2+l_{22})\sin(\delta_{22})+2b_1\sin(\delta_{22}+\theta_1)+t_{22}\cos(\delta_{22})}{2R} & \frac{-2(a_2+l_{22})\sin(\delta_{22})-2b_1\sin(\delta_{22}+\theta_1)+t_{22}\cos(\delta_{22})}{2R} \\
-\frac{2(a_2+l_{22})\sin(\delta_{22})+t_{22}\cos(\delta_{22})}{2R} & \frac{t_{22}\cos(\delta_{22})-2(a_2+l_{22})\sin(\delta_{22})}{2R} \\
0 & 0 \\
0 & 0
\end{array}$$

$$\begin{array}{cc}
\frac{\cos(\delta_{23}+\theta_1)}{R} & \frac{\cos(\delta_{23}+\theta_1)}{R} \\
\frac{\sin(\delta_{23}+\theta_1)}{R} & \frac{\sin(\delta_{23}+\theta_1)}{R} \\
-\frac{2(a_2+l_{23})\sin(\delta_{23})+2b_1\sin(\delta_{23}+\theta_1)+t_{23}\cos(\delta_{23})}{2R} & \frac{-2(a_2+l_{23})\sin(\delta_{23})-2b_1\sin(\delta_{23}+\theta_1)+t_{23}\cos(\delta_{23})}{2R} \\
-\frac{2(a_2+l_{23})\sin(\delta_{23})+t_{23}\cos(\delta_{23})}{2R} & \frac{t_{23}\cos(\delta_{23})-2(a_2+l_{23})\sin(\delta_{23})}{2R} \\
0 & 0 \\
0 & 0
\end{array}$$

$$\begin{array}{cc}
-2\mathrm{C}\alpha_{21}\sin(\delta_{21}+\theta_1) & -2\mathrm{C}\alpha_{22}\sin(\delta_{22}+\theta_1) \\
2\mathrm{C}\alpha_{21}\cos(\delta_{21}+\theta_1) & 2\mathrm{C}\alpha_{22}\cos(\delta_{22}+\theta_1) \\
-2\mathrm{C}\alpha_{21}((a_2+l_{21})\cos(\delta_{21})+b_1\cos(\delta_{21}+\theta_1)) & -2\mathrm{C}\alpha_{22}((a_2+l_{22})\cos(\delta_{22})+b_1\cos(\delta_{22}+\theta_1)) \\
-2\alpha_{21}(a_2+l_{21})\cos(\delta_{21}) & -2\mathrm{C}\alpha_{22}(a_2+l_{22})\cos(\delta_{22}) \\
0 & 0 \\
0 & 0
\end{array}$$

$$\begin{matrix} -2\mathrm{C}\alpha_{23}\sin(\delta_{23}+\theta_1) \\ 2\mathrm{C}\alpha_{23}\cos(\delta_{23}+\theta_1) \\ -2\mathrm{C}\alpha_{23}((a_2+\mathrm{l}23)\cos(\delta_{23})+b_1\cos(\delta_{23}+\theta_1)) \\ -2\mathrm{C}\alpha_{23}(a_2+l_{23})\cos(\delta_{23}) \\ 0 \\ 0 \end{matrix} \quad \begin{matrix} \frac{\cos(\delta_{31}+\theta_1+\theta_2)}{R} \\ \frac{\sin(\delta_{31}+\theta_1+\theta_2)}{R} \\ -\frac{2((a_2+b_2)\sin(\delta_{31}+\theta_2)+(a3-l_{31})\sin(\delta_{31})+b_1\sin(\delta_{31}+\theta_1+\theta_2))+t_{31}\cos(\delta_{31})}{2R} \\ -\frac{2(a_2+b_2)\sin(\delta_{31}+\theta_2)+2(a_3-l_{31})\sin(\delta_{31})+t_{31}\cos(\delta_{31})}{2R} \\ -\frac{2(a_3-l_{31})\sin(\delta_{31})+t_{31}\cos(\delta_{31})}{2R} \\ 0 \end{matrix}$$

$$\begin{matrix} \frac{\cos(\delta_{31}+\theta_1+\theta_2)}{R} \\ \frac{\sin(\delta_{31}+\theta_1+\theta_2)}{R} \\ \frac{t_{31}\cos(\delta_{31})-2((a_2+b_2)\sin(\delta_{31}+\theta 2)+(a_3-l_{31})\sin(\delta_{31})+b_1\sin(\delta_{31}+\theta_1+\theta_2))}{2R} \\ \frac{-2(a_2+b_2)\sin(\delta_{31}+\theta 2)+2(l_{31}-a_3)\sin(\delta_{31})+t_{31}\cos(\delta_{31})}{2R} \\ \frac{2(l_{31}-a_3)\sin(\delta_{31})+t_{31}\cos(\delta_{31})}{2R} \\ 0 \end{matrix}$$

$$\begin{matrix} \frac{\cos(\delta_{32}+\theta_1+\theta_2)}{R} \\ \frac{\sin(\delta_{32}+\theta_1+\theta_2)}{R} \\ -\frac{2((a_2+b_2)\sin(\delta_{32}+\theta_2)+(a_3+l_{32})\sin(\delta_{32})+b_1\sin(\delta_{32}+\theta_1+\theta_2))+t_{32}\cos(\delta_{32})}{2R} \\ -\frac{2(a_2+b_2)\sin(\delta_{32}+\theta_2)+2(a_3+l_{32})\sin(\delta_{32})+t_{32}\cos(\delta_{32})}{2R} \\ -\frac{2(a_3+l_{32})\sin(\delta_{32})+t_{32}\cos(\delta_{32})}{2R} \\ 0 \end{matrix}$$

$$\begin{matrix} \frac{\cos(\delta_{32}+\theta_1+\theta_2)}{R} \\ \frac{\sin(\delta_{32}+\theta_1+\theta_2)}{R} \\ \frac{t_{32}\cos(\delta_{32})-2((a_2+b_2)\sin(\delta_{32}+\theta_2)+(a_3+l_{32})\sin(\delta_{32})+b_1\sin(\delta_{32}+\theta_1+\theta_2))}{2R} \\ \frac{-2(a_2+b_2)\sin(\delta_{32}+\theta_2)-2(a_3+l_{32})\sin(\delta_{32})+t_{32}\cos(\delta_{32})}{2R} \\ \frac{t_{32}\cos(\delta_{32})-2(a_3+l_{32})\sin(\delta_{32})}{2R} \\ 0 \end{matrix}$$

$$\begin{matrix} -2\mathrm{C}\alpha_{31}\sin(\delta_{31}+\theta_1+\theta_2) \\ 2\mathrm{C}\alpha_{31}\cos(\delta_{31}+\theta_1+\theta_2) \\ -2\mathrm{C}\alpha_{31}((a_2+b_2)\cos(\delta_{31}+\theta_2)+(a_3-l_{31})\cos(\delta_{31})+b_1\cos(\delta_{31}+\theta_1+\theta_2)) \\ -2\mathrm{C}\alpha_{31}((a_2+b_2)\cos(\delta_{31}+\theta_2)+(a_3-l_{31})\cos(\delta_{31})) \\ 2\mathrm{C}\alpha_{31}(l_{31}-a_3)\cos(\delta_{31}) \\ 0 \end{matrix}$$

$$\begin{matrix} -2\mathrm{C}\alpha_{32}\sin(\delta_{32}+\theta_1+\theta_2) \\ 2\mathrm{C}\alpha_{32}\cos(\delta_{32}+\theta_1+\theta_2) \\ -2\mathrm{C}\alpha_{32}((a_2+b_2)\cos(\delta_{32}+\theta_2)+(a_3+l_{32})\cos(\delta_{32})+b_1\cos(\delta_{32}+\theta_1+\theta_2)) \\ -2\mathrm{C}\alpha_{32}((a_2+b_2)\cos(\delta_{32}+\theta_2)+(a_3+l_{32})\cos(\delta_{32})) \\ -2\mathrm{C}\alpha_{32}(a_3+l_{32})\cos(\delta_{32}) \\ 0 \end{matrix}$$

$$\begin{gathered}
\frac{\cos(\delta_{41}+\theta_1+\theta_2+\theta_3)}{R} \\
\frac{\sin(\delta_{41}+\theta_1+\theta_2+\theta_3)}{R} \\
-\frac{2((a_2+b_2)\sin(\delta_{41}+\theta_2+\theta_3)+(a_3+b_3)\sin(\delta_{41}+\theta_3)+(a_4+l_{41})\sin(\delta_{41})+b_1\sin(\delta_{41}+\theta_1+\theta_2+\theta_3))+t_{41}\cos(\delta_{41})}{2R} \\
-\frac{2((a_2+b_2)\sin(\delta_{41}+\theta_2+\theta_2)+(a_3+b_3)\sin(\delta_{41}+\theta_3)+(a_4+l_{41})\sin(\delta_{41}))+t_{41}\cos(\delta_{41})}{2R} \\
-\frac{2(a_3+b_3)\sin(\delta_{41}+\theta_3)+2(a_4+l_{41})\sin(\delta_{41})+t_{41}\cos(\delta_{41})}{2R} \\
-\frac{2(a_4+l_{41})\sin(\delta_{41})+t_{41}\cos(\delta_{41})}{2R}
\end{gathered}$$

$$\begin{gathered}
\frac{\cos(\delta_{41}+\theta_1+\theta_2+\theta_3)}{R} \\
\frac{\sin(\delta_{41}+\theta_1+\theta_2+\theta_3)}{R} \\
\frac{t_{41}\cos(\delta_{41})-2((a_2+b_2)\sin(\delta_{41}+\theta_2+\theta_3)+(a_3+b_3)\sin(\delta_{41}+\theta_3)+(a_4+l_{41})\sin(\delta_{41})+b_1\sin(\delta_{41}+\theta_1+\theta_2+\theta_3))}{2R} \\
\frac{t_{41}\cos(\delta_{41})-2((a_2+b_2)\sin(\delta_{41}+\theta_2+\theta_3)+(a_3+b_3)\sin(\delta_{41}+\theta_3)+(a_4+l_{41})\sin(\delta_{41}))}{2R} \\
\frac{-2(a_3+b_3)\sin(\delta_{41}+\theta_3)-2(a_4+l_{41})\sin(\delta_{41})+t_{41}\cos(\delta_{41})}{2R} \\
\frac{t_{41}\cos(\delta_{41})-2(a_4+l_{41})\sin(\delta_{41})}{2R}
\end{gathered}$$

$$\begin{gathered}
\frac{\cos(\delta_{42}+\theta_1+\theta_2+\theta_3)}{R} \\
\frac{\sin(\delta_{42}+\theta_1+\theta_2+\theta_3)}{R} \\
-\frac{2((a_2+b_2)\sin(\delta_{42}+\theta_2+\theta_3)+(a_3+b_3)\sin(\delta_{42}+\theta_3)+(a_4+l_{42})\sin(\delta_{42})+b_1\sin(\delta_{42}+\theta_1+\theta_2+\theta_3))+t_{42}\cos(\delta_{42})}{2R} \\
-\frac{2((a_2+b_2)\sin(\delta_{42}+\theta_2+\theta_3)+(a_3+b_3)\sin(\delta_{42}+\theta_3)+(a_4+l_{42})\sin(\delta_{42}))+t_{42}\cos(\delta_{42})}{2R} \\
-\frac{2(a_3+b_3)\sin(\delta_{42}+\theta_3)+2(a_4+l_{42})\sin(\delta_{42})+t_{42}\cos(\delta_{42})}{2R} \\
-\frac{2(a_4+l_{42})\sin(\delta_{42})+t_{42}\cos(\delta_{42})}{2R}
\end{gathered}$$

$$\begin{gathered}
\frac{\cos(\delta_{42}+\theta_1+\theta_2+\theta_3)}{R} \\
\frac{\sin(\delta_{42}+\theta_1+\theta_2+\theta_3)}{R} \\
\frac{t_{42}\cos(\delta_{42})-2((a_2+b_2)\sin(\delta_{42}+\theta_2+\theta_3)+(a_3+b_3)\sin(\delta_{42}+\theta_3)+(a_4+l_{42})\sin(\delta_{42})+b_1\sin(\delta_{42}+\theta_1+\theta_2+\theta_3))}{2R} \\
\frac{t_{42}\cos(\delta_{42})-2((a_2+b_2)\sin(\delta_{42}+\theta_2+\theta_3)+(a_3+b_3)\sin(\delta_{42}+\theta_3)+(a_4+l_{42})\sin(\delta_{42}))}{2R} \\
\frac{-2(a_3+b_3)\sin(\delta_{42}+\theta_3)-2(a_4+l_{42})\sin(\delta_{42})+t_{42}\cos(\delta_{42})}{2R} \\
\frac{t_{42}\cos(\delta_{42})-2(a_4+l_{42})\sin(\delta_{42})}{2R}
\end{gathered}$$

$$\begin{gathered}
\frac{\cos(\delta_{43}+\theta_1+\theta_2+\theta_3)}{R} \\
\frac{\sin(\delta_{43}+\theta_1+\theta_2+\theta_3)}{R} \\
-\frac{2((a_2+b_2)\sin(\delta_{43}+\theta_2+\theta_3)+(a_3+b_3)\sin(\delta_{43}+\theta_3)+(a_4+l_{43})\sin(\delta_{43})+b_1\sin(\delta_{43}+\theta_1+\theta_2+\theta_3))+t_{43}\cos(\delta_{43})}{2R} \\
-\frac{2((a_2+b_2)\sin(\delta_{43}+\theta_2+\theta_3)+(a_3+b_3)\sin(\delta_{43}+\theta_3)+(a_4+l_{43})\sin(\delta_{43}))+t_{43}\cos(\delta_{43})}{2R} \\
-\frac{2(a_3+b_3)\sin(\delta_{43}+\theta_3)+2(a_4+l_{43})\sin(\delta_{43})+t_{43}\cos(\delta_{43})}{2R} \\
-\frac{2(a_4+l_{43})\sin(\delta_{43})+t_{43}\cos(\delta_{43})}{2R}
\end{gathered}$$

$$\begin{gathered}
\frac{\cos(\delta_{43}+\theta_1+\theta_2+\theta_3)}{R} \\
\frac{\sin(\delta_{43}+\theta_1+\theta_2+\theta_3)}{R} \\
\frac{t_{43}\cos(\delta_{43})-2((a_2+b_2)\sin(\delta_{43}+\theta_2+\theta_3)+(a_3+b_3)\sin(\delta_{43}+\theta_3)+(a_4+l_{43})\sin(\delta_{43})+b_1\sin(\delta_{43}+\theta_1+\theta_2+\theta_3))}{2R} \\
\frac{t_{43}\cos(\delta_{43})-2((a_2+b_2)\sin(\delta_{43}+\theta_2+\theta_3)+(a_3+b_3)\sin(\delta_{43}+\theta_3)+(a_4+l_{43})\sin(\delta_{43}))}{2R} \\
\frac{-2(a_3+b_3)\sin(\delta_{43}+\theta_3)-2(a_4+l_{43})\sin(\delta_{43})+t_{43}\cos(\delta_{43})}{2R} \\
\frac{t_{43}\cos(\delta_{43})-2(a_4+l_{43})\sin(\delta_{43})}{2R}
\end{gathered}$$

$$
\begin{array}{c}
-2\mathrm{C}\alpha_{41}\sin(\delta_{41}+\theta_1+\theta_2+\theta_3)\\
2\mathrm{C}\alpha_{41}\cos(\delta_{41}+\theta_1+\theta_2+\theta_3)\\
-2\mathrm{C}\alpha_{41}((a_2+b_2)\cos(\delta_{41}+\theta_2+\theta_2)+(a_3+b_3)\cos(\delta_{41}+\theta_3)+(a_4+l_{41})\cos(\delta_{41})+b_1\cos(\delta_{41}+\theta_1+\theta_2+\theta_3))\\
-2\mathrm{C}\alpha_{41}((a_2+b_2)\cos(\delta_{41}+\theta_2+\theta_3)+(a_3+b_3)\cos(\delta_{41}+\theta_3)+(a_4+l_{41})\cos(\delta_{41}))\\
-2\mathrm{C}\alpha_{41}((a_3+b_3)\cos(\delta_{41}+\theta_3)+(a_4+l_{41})\cos(\delta_{41}))\\
-2\mathrm{C}\alpha_{41}(a_4+l_{41})\cos(\delta_{41})
\end{array}
$$

$$
\begin{array}{c}
-2\mathrm{C}\alpha_{42}\sin(\delta_{42}+\theta_1+\theta_2+\theta_3)\\
2\mathrm{C}\alpha_{42}\cos(\delta_{42}+\theta_1+\theta_2+\theta_3)\\
-2\mathrm{C}\alpha_{42}((a_2+b_2)\cos(\delta_{42}+\theta_2+\theta_3)+(a_3+b_3)\cos(\delta_{42}+\theta_3)+(a_4+l_{42})\cos(\delta_{42})+b_1\cos(\delta_{42}+\theta_1+\theta_2+\theta_3))\\
-2\mathrm{C}\alpha_{42}((a_2+b_2)\cos(\delta_{42}+\theta_2+\theta_3)+(a_3+b_3)\cos(\delta_{42}+\theta_3)+(a_4+l_{42})\cos(\delta_{42}))\\
-2\mathrm{C}\alpha_{42}((a_3+b_3)\cos(\delta_{42}+\theta_3)+(a_4+l_{42})\cos(\delta_{42}))\\
-2\mathrm{C}\alpha_{42}(a_4+l_{42})\cos(\delta_{42})
\end{array}
$$

$$
\left.
\begin{array}{c}
-2\mathrm{C}\alpha_{43}\sin(\delta_{43}+\theta_1+\theta_2+\theta_3)\\
2\mathrm{C}\alpha_{43}\cos(\delta_{43}+\theta_1+\theta_2+\theta_3)\\
-2\mathrm{C}\alpha_{43}((a_2+b_2)\cos(\delta_{43}+\theta_2+\theta_3)+(a_3+b_3)\cos(\delta_{43}+\theta_3)+(a_4+l_{43})\cos(\delta_{43})+b_1\cos(\delta_{43}+\theta_1+\theta_2+\theta_3))\\
-2\mathrm{C}\alpha_{43}((a_2+b_2)\cos(\delta_{43}+\theta_2+\theta3)+(a_3+b_3)\cos(\delta_{43}+\theta_3)+(a_4+l_{43})\cos(\delta_{43}))\\
-2\mathrm{C}\alpha_{43}((a_3+b_3)\cos(\delta_{43}+\theta_3)+(a_4+l_{43})\cos(\delta_{43}))\\
-2\mathrm{C}\alpha_{43}(a_4+l_{43})\cos(\delta_{43})
\end{array}
\right)
$$

A.3 Model parameters

The model parameters used in the simulations for the A-double are given by Volvo in the VTM-model or approximated given the information in [16]. In the VTM-model a very complex tire model is used, which does not use a linear model including cornering stiffness. For the control allocation, the approximation of a linear lateral tire model in (2.4), needs an estimation of the cornering stiffness. Provided by Volvo, the cornering stiffness for the front axle and rear axles (all other axles) are estimated according to

$$\begin{cases} C_{\alpha,front} = 6.85 m_a g \\ C_{\alpha,rear} = 16.17 m_a g \end{cases} \tag{A.5}$$

where m_a is the axle load on the specific axle and g is the gravitational constant. The notation used in the following is the same as used throughout the report. For example x_{ji}, means for unit j and axle i. Only some parameters used in the VTM-model are presented here, the rest can be found in the initialization files. For convenience, longitudinal lengths are defined with sign conversion, positive signs for positions in front of CoG of the unit, and negative signs for positions behind CoG of the unit. The parameters used for the tractor-semitrailer have some minor differences to the A-double, due to another setup in the VTM-model, and are not presented here. The model parameters used in the simulations for the A-double combination are given in Table A.1.

Table A.1: Model parameters for the A-double combination

Parameter	**Symbol**	**Value**	**Unit**
Axle load, unit 1, axle 1	m_{a11}	7063	[kg]
Axle load, unit 1, axle 2	m_{a12}	8535	[kg]
Axle load, unit 1, axle 3	m_{a13}	8535	[kg]
Axle load, unit 2, axle 1	m_{a21}	6436	[kg]
Axle load, unit 2, axle 2	m_{a22}	6436	[kg]
Axle load, unit 2, axle 3	m_{a23}	6436	[kg]
Axle load, unit 3, axle 1	m_{a31}	8044	[kg]
Axle load, unit 3, axle 2	m_{a32}	8044	[kg]
Axle load, unit 4, axle 1	m_{a41}	6804	[kg]
Axle load, unit 4, axle 2	m_{a42}	6804	[kg]
Axle load, unit 4, axle 3	m_{a43}	6804	[kg]
Cornering stiffness, unit 1, axle 1	$C_{\alpha 11}$	237 330	[N/rad]
Cornering stiffness, unit 1, axle 2	$C_{\alpha 12}$	676 950	[N/rad]
Cornering stiffness, unit 1, axle 3	$C_{\alpha 13}$	676 950	[N/rad]
Cornering stiffness, unit 2, axle 1	$C_{\alpha 21}$	510 470	[N/rad]
Cornering stiffness, unit 2, axle 2	$C_{\alpha 22}$	510 470	[N/rad]
Cornering stiffness, unit 2, axle 3	$C_{\alpha 23}$	510 470	[N/rad]
Cornering stiffness, unit 3, axle 1	$C_{\alpha 31}$	638 000	[N/rad]
Cornering stiffness, unit 3, axle 2	$C_{\alpha 32}$	638 000	[N/rad]
Cornering stiffness, unit 4, axle 1	$C_{\alpha 41}$	539 650	[N/rad]
Cornering stiffness, unit 4, axle 2	$C_{\alpha 42}$	539 650	[N/rad]
Cornering stiffness, unit 4, axle 3	$C_{\alpha 43}$	539 650	[N/rad]
Distance from CoG to coupling point front, unit 2	a_2	4.43	[m]
Distance from CoG to coupling point front, unit 3	a_3	4.55	[m]

Parameter	**Symbol**	**Value**	**Unit**
Distance from CoG to coupling point front, unit 4	a_4	4.65	[m]
Distance from CoG to coupling point rear, unit 1	b_1	-1.95	[m]
Distance from CoG to coupling point rear, unit 2	b_2	-4	[m]
Distance from CoG to coupling point rear, unit 3	b_3	0	[m]
Distance from CoG to axle 1, unit 1	l_{11}	1.45	[m]
Distance from CoG to axle 2, unit 1	l_{12}	-1.55	[m]
Distance from CoG to axle 3, unit 1	l_{13}	-2.86	[m]
Distance from CoG to axle 1, unit 2	l_{21}	-1.97	[m]
Distance from CoG to axle 2, unit 2	l_{22}	-3.27	[m]
Distance from CoG to axle 3, unit 2	l_{23}	-4.57	[m]
Distance from CoG to axle 1, unit 3	l_{31}	0.65	[m]
Distance from CoG to axle 2, unit 3	l_{32}	-0.65	[m]
Distance from CoG to axle 1, unit 4	l_{41}	-1.75	[m]
Distance from CoG to axle 2, unit 4	l_{42}	-3.05	[m]
Distance from CoG to axle 3, unit 4	l_{43}	-4.35	[m]
Height to CoG over ground, sprung mass, front, unit 1	h_{01}	0.80	[m]
Height to CoG over ground, sprung mass, front, unit 2	h_{02}	1.51	[m]
Height to CoG over ground, sprung mass, front, unit 3	h_{03}	0.90	[m]
Height to CoG over ground, sprung mass, front, unit 4	h_{04}	1.54	[m]
Yaw mass moment of inertia, unit 1	J_1	20 000	[kgm^2]
Yaw mass moment of inertia, unit 2	J_2	543 000	[kgm^2]
Yaw mass moment of inertia, unit 3	J_3	2 000	[kgm^2]
Yaw mass moment of inertia, unit 4	J_4	546 000	[kgm^2]
Mass, unit 1	m_1	24 134	[kg]

Parameter	**Symbol**	**Value**	**Unit**
Mass, unit 2	m_2	19 308	[kg]
Mass, unit 3	m_3	16 088	[kg]
Mass, unit 4	m_4	20 412	[kg]
Wheel radius	R	0.5	[m]
Track width, axle 1, unit 1	t_{11}	2.05	[m]
Track width, axle 2, unit 1	t_{12}	1.85	[m]
Track width, axle 3, unit 1	t_{13}	1.85	[m]
Track width, axle 1, unit 2	t_{21}	2.05	[m]
Track width, axle 2, unit 2	t_{22}	2.05	[m]
Track width, axle 3, unit 2	t_{23}	2.05	[m]
Track width, axle 1, unit 3	t_{31}	2.05	[m]
Track width, axle 2, unit 3	t_{32}	2.05	[m]
Track width, axle 1, unit 4	t_{41}	2.05	[m]
Track width, axle 2, unit 4	t_{42}	2.05	[m]
Track width, axle 3, unit 4	t_{43}	2.05	[m]

A.4 Simulation results

A.4.1 Split friction braking

Tire forces for the simulation of Vehicle 4, where the low friction side is set to $\mu = 0.1$, are shown in the figures below. On the low friction side the tires are saturated and the linear tire model, which is assumed according to Figure 2.4, may not be enough to describe the tire dynamics. Even with this uncertainty, the control structure produces reasonable results.

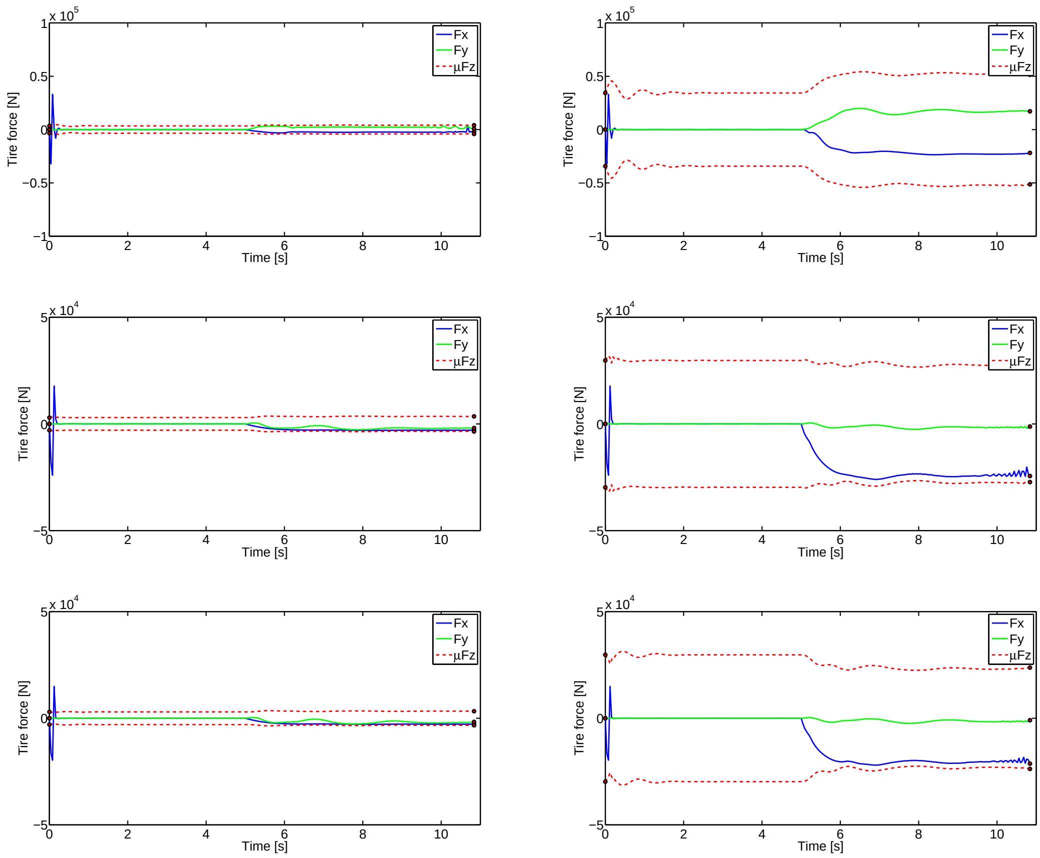

Figure A.1: Tire forces for Vehicle 4 - Unit 1. Upper left: Tire 11 left. Upper right: Tire 11 right. Middle left: Tire 12 left. Middle right: Tire 12 right. Lower left: Tire 13 left. Lower right: Tire 13 right.

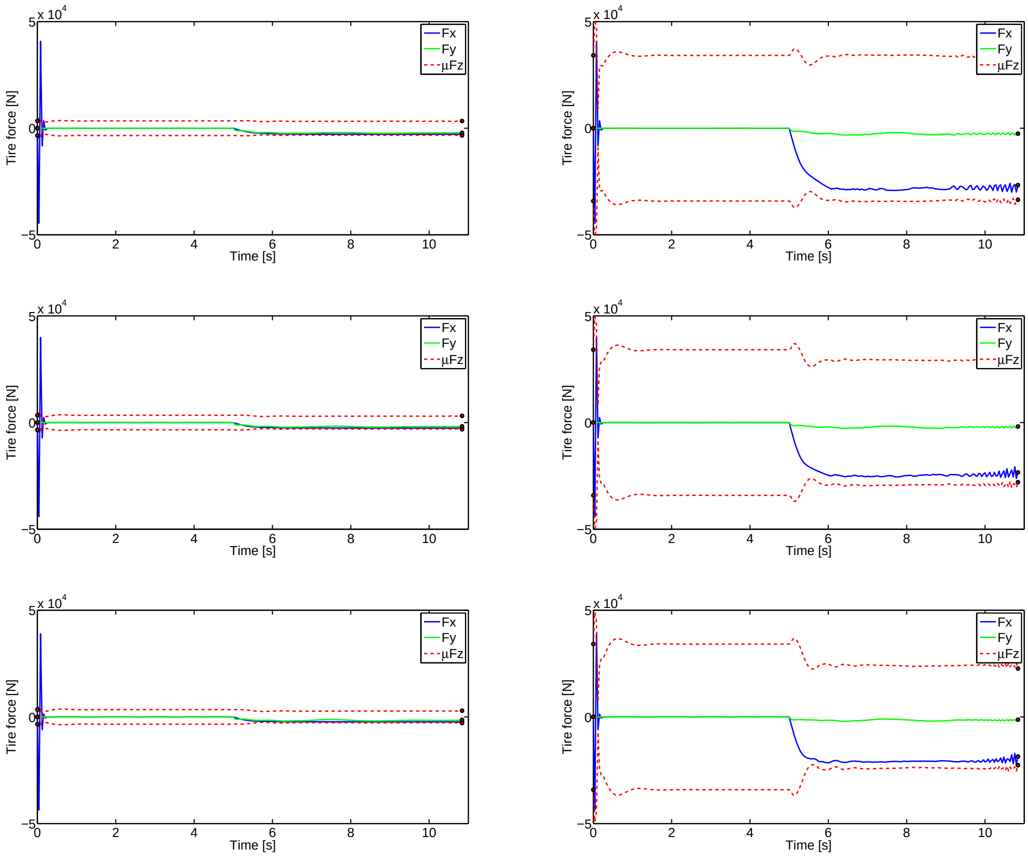

Figure A.2: Tire forces for Vehicle 4 - Unit 2. Upper left: Tire 21 left. Upper right: Tire 21 right. Middle left: Tire 22 left. Middle right: Tire 22 right. Lower left: Tire 23 left. Lower right: Tire 23 right.

A.4.2 Single lane change

Tire forces for the simulation of Vehicle 5 are shown in the figures below. There is a large marginal between the lateral forces and the maximum available force μF_z. The assumption of a linear lateral tire model, according to Figure 2.4, could be considered as a good approximation.

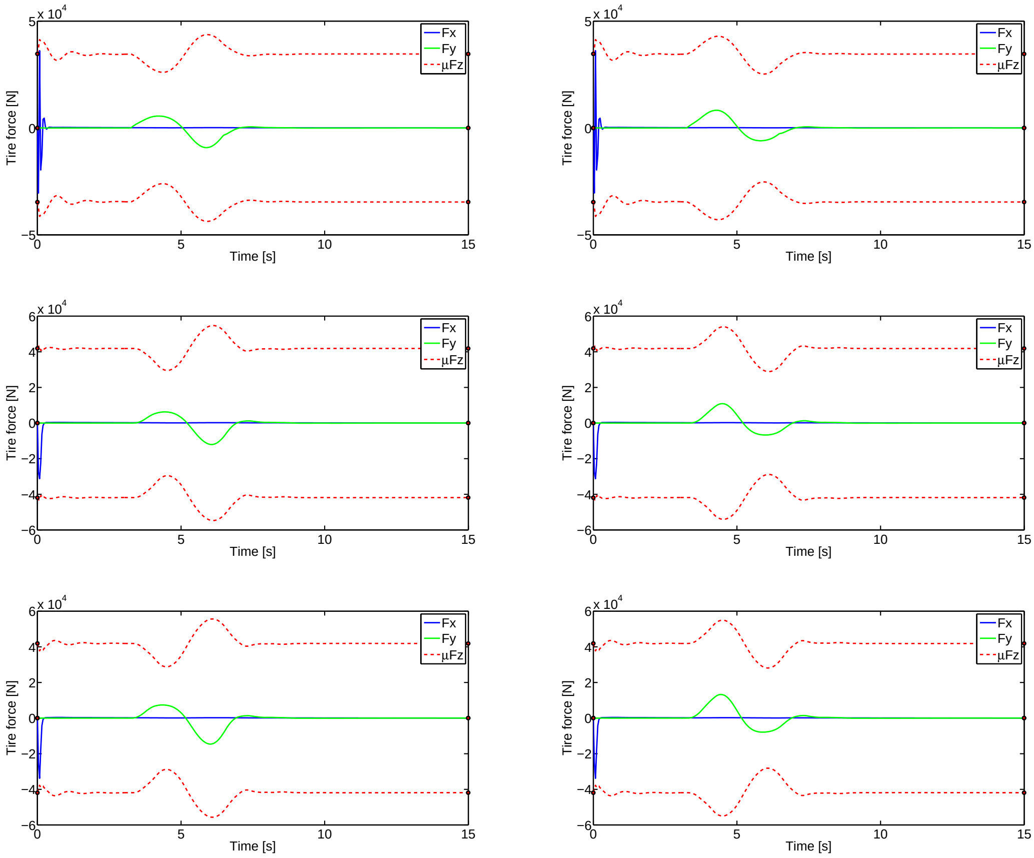

Figure A.3: Tire forces for Vehicle 5 - Unit 1. Upper left: Tire 11 left. Upper right: Tire 11 right. Middle left: Tire 12 left. Middle right: Tire 12 right. Lower left: Tire 13 left. Lower right: Tire 13 right.

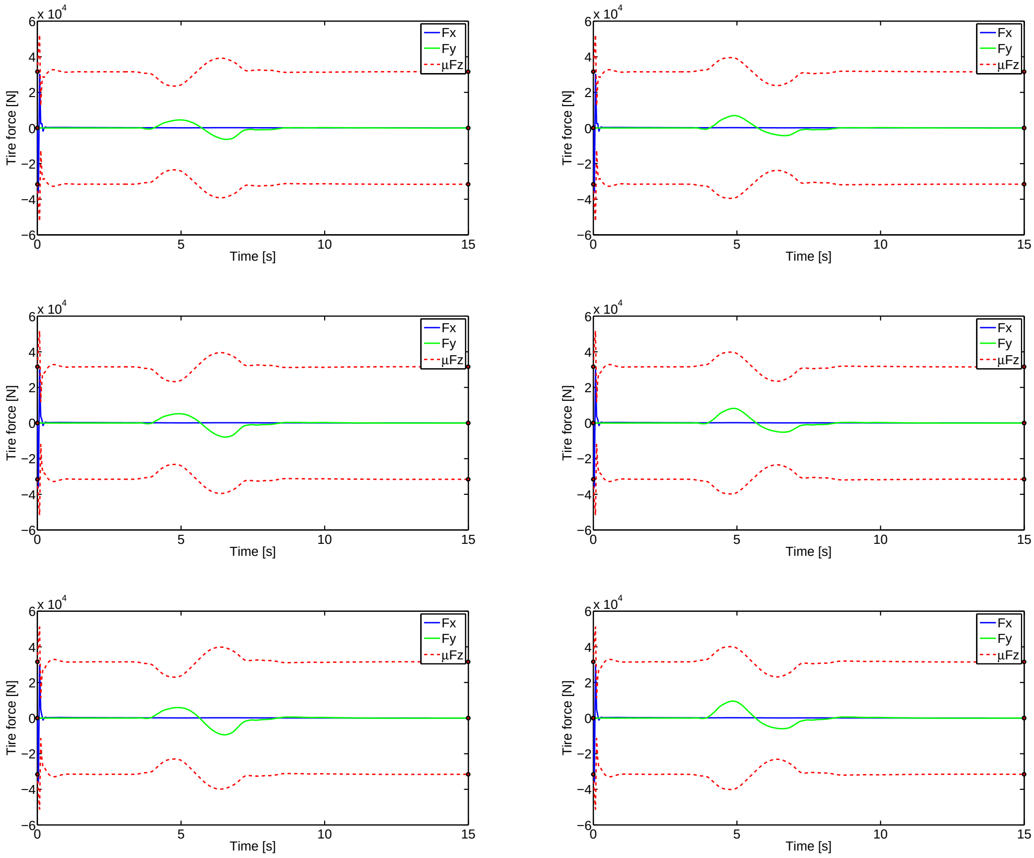

Figure A.4: Tire forces for Vehicle 5 - Unit 2. Upper left: Tire 21 left. Upper right: Tire 21 right. Middle left: Tire 22 left. Middle right: Tire 22 right. Lower left: Tire 23 left. Lower right: Tire 23 right.

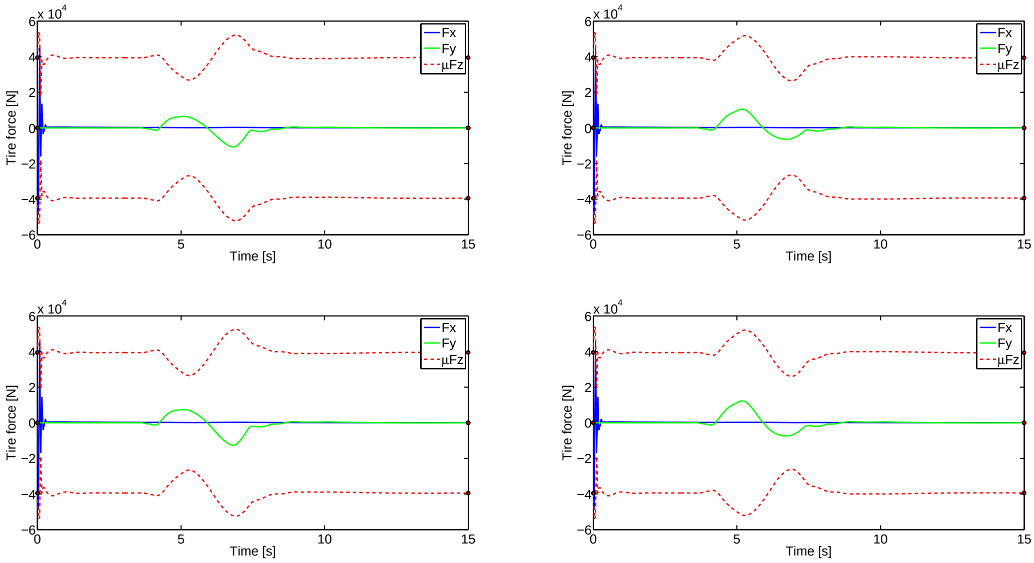

Figure A.5: Tire forces for Vehicle 5 - Unit 3. Upper left: Tire 31 left. Upper right: Tire 31 right. Lower left: Tire 32 left. Lower right: Tire 32 right.

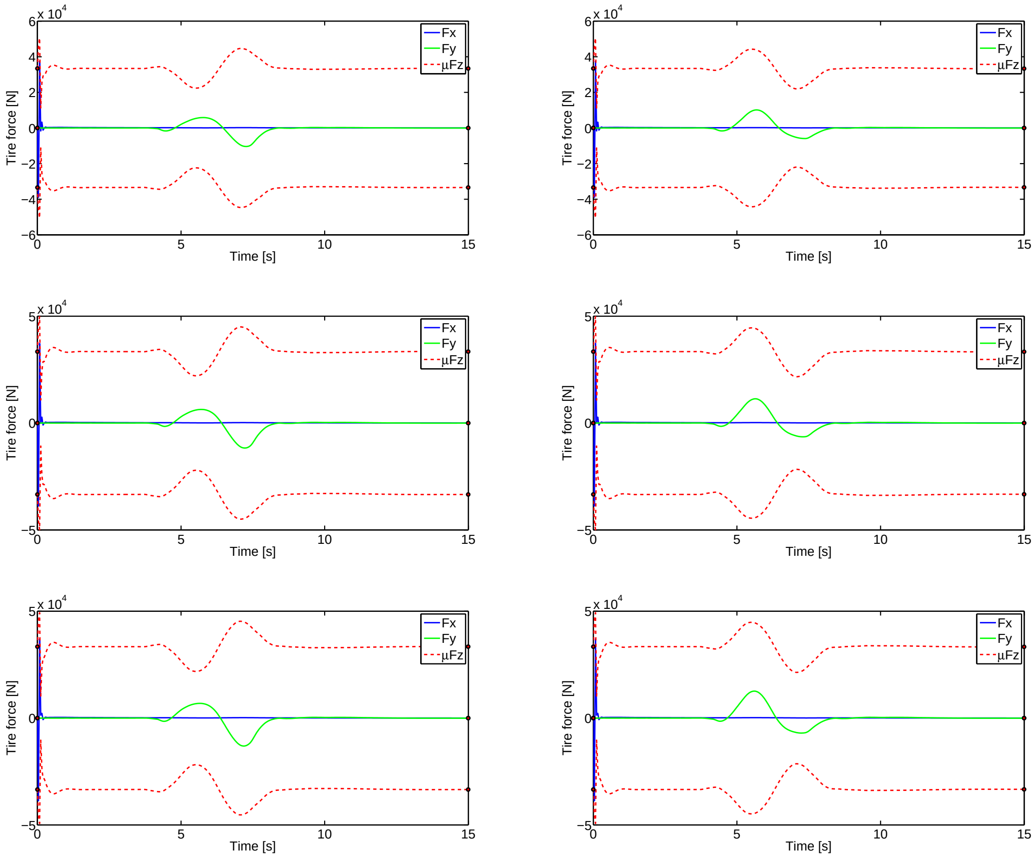

Figure A.6: Tire forces for Vehicle 5 - Unit 4. Upper left: Tire 41 left. Upper right: Tire 41 right. Middle left: Tire 42 left. Middle right: Tire 42 right. Lower left: Tire 43 left. Lower right: Tire 43 right.